ELSEVIER

Colloids and Surfaces
A: Physicochemical and Engineering Aspects 202 (2002) 243–267

COLLOIDS AND SURFACES A

www.elsevier.com/locate/colsurfa

Two-dimensional synthesis of anisotropic nanoparticles

Gennady B. Khomutov *

Faculty of Physics, Moscow State University, Vorobjevy Gory, 119899 Moscow, Russia

Received 5 April 2001; accepted 31 July 2001

Abstract

A novel approach for the synthesis of nanoparticles has been introduced in which nanoparticles are fabricated via decomposition of an insoluble precursor compound in a monolayer at the gas/liquid interface, and nanoparticle growth is an example of a two-dimensional (2-D) process where true 2-D diffusion of precursor molecules, active intermediates, metal atoms and its complexes, nucleus and growing nanoparticles, surfactants and additives occurs only in the plain of the monolayer. In the present contribution, two possible example embodiments of the approach are described. First, magnetic iron-containing nanoparticles were photochemically generated by the ultraviolet decomposition of a volatile precursor compound iron pentacarbonyl in a mixed Langmuir monolayer. Secondly, nanoparticles were produced by the chemical reduction of palladium from $Pd_3(CH_3COO)_6$ molecules and of gold from $Au(P(C_6H_5)_3)Cl$ in the mixed monolayers. Stearic acid, arachidic acid or octadecyl amine were used as surfactants to form Langmuir monolayers on the aqueous sub-phase surface and to stabilize the growing nanoparticles. Nanoparticles were formed in the 2-D gas phase of a monolayer (at very low or no surface pressure). The morphology of the nanoparticles synthesized was characterized by atomic force microscopy and transmission electron microscopy. It was established that the shape, size and crystallinity of the resulting nanoparticles were dependent substantially on the monolayer composition and state during the growth process. It was demonstrated that the shape of the magnetic nanoparticles can be changed from 2-D isotropic plate and ring-like to the field-aligned ellipsoidal and needle-like when external magnetic field parallel to the plane of particulate monolayer was applied during the synthesis. The effects of self-organization of nanoparticles and formation of 2-D nanostructures are also presented. It is shown that controlling the mixed monolayer composition and compression state opens wide possibilities for the growth regulation of the 2-D growth of nanoparticles and self-organization processes to obtain inorganic nanostructures with various and unique morphologies.

Keywords: Nanoparticles; Langmuir monolayer; Synthesis; Self-organization; Applied field; Nanotechnology

1. Introduction

Development of novel nanofabrication techniques and methods to control effectively the interactions, structure and morphology, arrangement and patterning at the nanoscopic length scale is currently of principal importance in nanotechnology, materials research and in designing new advanced nanostructured and functionalized materials and films with pre-determined and unique properties what offers the prospects for

* Tel.: +7-95-939-3007; fax: +7-95-939-1195.
E-mail address: gbk@phys.msu.su (G.B. Khomutov).

0927-7757/02/$ - see front matter
PII: S0927-7757(01)01079-2

major technological advances in a wide variety of systems. Nanoparticles and nanostructured materials are a subject of growing interest due to their unique electronic, optical, magnetic, chemical and mechanical properties important for fundamental studies and wide range of technological applications [1–5]. Nanophase materials and nanoparticle-based nanostructures play a key role in research and development works directed to the creation of nanoscale structural and functional elements for information processing and storage technologies (particularly, magnetic storage), advanced electronics, optics, chemistry (catalysis, new composite and nanostructured materials), biotechnologies and many others where the principal role of nanomaterials is now recognized. The preparation of nanoparticles and nanoparticulate condensed and liquid composite materials has become a major research and technology area in nanoscale science and engineering. Many methods are known to synthesize inorganic sub-micron particles, and properties of the resulted product, particularly size, shape, polydispersity, crystal morphology and degree of crystallinity are usually dependent on the nanoparticle composition and reaction conditions. Various colloidal techniques such as normal/reverse micelle method [6,7], double emulsion [8,9], Langmuir monolayer technique [10], and the two-phase liquid–liquid systems [11], were exploited to prepare metallic and semiconducting nanoparticles. When inorganic nanoparticles were generated at the gas/liquid interfaces with surfactant Langmuir monolayers used as templates, the initial reagents were located in a gas and/or liquid phases and the growth process was predominantly of a three-dimensional (3-D) character [12–15]. Interesting effects of surfactant-dependent controlled oriented crystallization were discovered in such systems [14,16]. Organometallic techniques, e.g. decomposition of volatile organometallic precursors such as transition metal carbonyls (in particular, iron pentacarbonyl $Fe(CO)_5$) in the presence of different surface-active compounds were used to produce colloidal suspensions of stabilized ultrafine metallic magnetic particles of quasi-spherical shape [17–23].

For basic studies and potential applications anisotropic nanoparticles are of particular interest because nanostructures and materials with such nanoparticles can exhibit novel and enhanced properties compared with the spherical nanoparticles what could open possibilities to realize new nanostructured systems and advanced materials with unique properties. The anisotropy of size-dependent characteristics of anisotropic nanoparticles and substantial surface effects can result in much more rich physical and chemical properties in comparison with the conventional isotropic spherical particles due to the anisotropy in electronic interactions and quantum confinement effects, magnetic anisotropy, etc. Also, ordered one-dimensional (1-D), two-dimensional (2-D) and three-dimensional (3-D) arrays and aggregates of anisotropic nanoparticles are of substantial interest due to the expectable new collective properties not encountered with isotropic nanoparticles and in connection with the development of effective nanoscale patterning methods based on self-assembly and self-organization effects.

Inorganic crystal nanoparticles can be naturally highly anisotropic in shape, e.g. acicular γ-phase iron oxide (γ-Fe_2O_3) and CrO_2 particles or hexagonal plate-like barium ferrite crystallites widely used in conventional magnetic recording media materials [24,25]. The conditions of bulk synthesis and surfactant nature often influence the properties of grown nanoparticles, particularly the shape, size, crystal morphology and degree of crystallinity [26–28]. Synthesis of nanoparticles in confined geometries, and in anisotropic and nanostructured reaction media can result in anisotropic and size-controlled inorganic nanoparticles [29,30]. Thus, synthesis in nanoporous material [31] and in anisotropic reverse micelles [32] gives prolate metallic nanoparticles. The use of multilayer Langmuir–Blodgett (LB) films as templates and metal–organic precursor matrix for the synthesis of inorganic nanoparticles in quasi-2-D organic nanoreactors resulted in oblate metallic [33] and semiconductor [34,35] nanoparticles. It was shown that heating treatment could change the size and shape of thiolate-encapsulated gold nanoparticles [36].

A novel approach towards the synthesis of nanoparticles was introduced recently by our group [37]. The idea of the approach is the formation of nanoparticles and nanostructures via 2-D growth process in a dynamic monomolecular structure at the gas/liquid interface. In this approach nanoparticles are fabricated via decomposition of an insoluble metal–organic precursor compound in a mixed amphiphile Langmuir monolayer at the gas/liquid interface, and nanoparticle growth is an example of the 2-D process where precursor molecules, active intermediates, metal atoms and complexes, nucleus and nanoparticles, surfactants and additives form a true monolayer reaction system at the liquid surface. The present work illustrates briefly some possible embodiments of the approach allowing the formation of highly anisotropic metal-containing nanoparticles with widely and controllably variable shape and morphology. In the experiments described in this contribution nanoparticles were generated by the ultraviolet (UV) decomposition of iron pentacarbonyl, and by the chemical reduction of palladium from metal–organic $Pd_3(CH_3COO)_6$ molecules and of gold from $Au(P(C_6H_5)_3)Cl$ in the mixed monolayers with stearic acid, arachidic acid or octadecyl amine on the surface of the aqueous phase. Because of the synthesis of nanoparticles in the present approach being carried out in a Langmuir monolayer at the gas/liquid interface, there is an opportunity to deposit monolayer or multilayer LB films with synthesized nanoparticles onto the atomically flat substrates (as mica or graphite) and to apply scanning probe microscopic techniques to investigate the topography of the resulting nanostructures with high-space resolution. Atomic force microscopy (AFM) was used earlier to study the morphology of fatty acid mono- and multilayer LB films [38]. It was established that domains can exist in such films with different heights and sizes, and height differences between domains corresponded to the step heights multiple to the thickness of a monolayer of vertically oriented surfactant molecules [38]. For the films obtained in the present work composed of surfactant molecules and synthesized nanoparticles where nanoparticles were probably covered by the surfactant layer the comparison structural data from AFM and transmission electron microscopy (TEM) were used to analyze the shape and morphology of the synthesized nanostructures.

2. Experimental

Stearic acid (SA), arachidic acid (AA) and octadecyl amine (ODA) were obtained from Aldrich/Sigma. Iron pentacarbonyl $Fe(CO)_5$ was obtained from Alfa Inorganic. $Pd_3(CH_3COO)_6$ and $Au(P(C_6H_5)_3)Cl$ were kindly supplied by Professor S.P. Gubin. All chemicals were used as received without further purification. Milli-Q water purification system was used to produce water with an average resistivity of 18 MΩ cm for all experiments. Fatty acids and long-chain amines are known as classical surfactant compounds to form insoluble Langmuir monolayers at the gas/aqueous phase interface [39]. At the same time such compounds are widely used as stabilizing agents to prevent aggregation of particles in colloidal suspensions (e.g. magnetic fluids [40]) due to the short-range steric repulsion between surfactant monolayers formed on the surface of colloid particles. In the 2-D synthesis method the properties of surfactants to form Langmuir monolayer and to passivate surface of clusters and nanoparticles can be combined successfully.

Experimentally, iron-containing magnetic nanoparticles were fabricated by the UV decomposition (UV irradiation from 300 mW conventional UV source, $\lambda \cong 300$ nm) of iron pentacarbonyl at the ambient temperature (21 °C) in a mixed monolayer formed by spreading an appropriate amount of the chloroform solution of iron pentacarbonyl with SA on the surface of purified water (pH 5.6). The lamp was held 25 cm above the monolayer delivering UV power of $\sim 500\ \mu W\ cm^{-2}$. $Fe(CO)_5$ is a volatile water-insoluble metal–organic compound widely used in the chemical vapor deposition technique, with gas phase CO and iron and/or iron oxycarbide species as final products, under normal conditions it is a liquid with a tendency to evaporate slowly. The surface pressure–monolayer area (π–A) isotherm of a pure SA monolayer was not

changed noticeably after UV-irradiation for 25 min. Spreading solutions were prepared by dissolving SA and iron pentacarbonyl in chloroform to give concentration of 1×10^{-4} M SA molecules. Initial $Fe(CO)_5$/SA ratio in a monolayer was varied from 10:1 to 1:1. UV exposure time was 6 s and 4 min, surface pressure in a mixed monolayer was varied controllably in different experiments.

To synthesize Pd and Au nanoparticles the mixed spreading solutions of $Pd_3(CH_3COO)_6$ or $Au(P(C_6H_5)_3)Cl$ with AA or ODA in chloroform were prepared (precursor/surfactant ratio was varied in different experiments). AA in these experiments was used due to its low solubility in water at high pH in comparison with SA. Spreading solution was then deposited onto the aqueous phase containing sodium borohydride as reducing agent ($NaBH_4$ concentration varied from 0.001 to 0.01 M). Nanoparticles then were synthesized in a mixed precursor and surfactant Langmuir monolayer formed after solvent evaporation on the surface of borohydride solution (incubation time 20 min).

Nanoparticles were formed in the 2-D gas phase of a monolayer (at very low or no surface pressure) where in-plane diffusion of monolayer compounds was allowed. Monolayers with synthesized nanoparticles were then compressed by a mobile Teflon barrier at a continuous barrier speed ~ 3 Å^2/molecule × min and deposited onto the solid substrate at a constant monolayer surface pressure $\pi \approx 25$ mN m^{-1} and ambient temperature (~ 21 °C) using the conventional vertical lifting method with good transfer ratios to form monolayer nanoparticulate samples for AFM and TEM measurements. The compression of a monolayer with growing nanoparticles to the monolayer solid state and following deposition onto the solid substrate stop the diffusion-mediated processes in the monolayer and fix effectively the synthesized nanoparticles. It was found that AFM and TEM images of the formed monolayer nanoparticulate samples were reproducible after a few months of storage under ambient conditions. Mica substrates were used for AFM investigations and were freshly cleaved immediately before monolayer deposition. Samples for TEM measurements were prepared by direct collection of nanoparticulate monolayer material from aqueous sub-phase surface onto the Formwar film supported by the copper grid (diameter = 3 mm), then samples were dried and subjected to TEM analyses. In this work the Langmuir monolayer formation, surface pressure–monolayer area isotherm measurements and monolayer transfer to the solid substrates were carried out on a full automatic conventional Teflon trough as described elsewhere [41]. Surface pressure was measured with Wilhelmy plate balance.

AFM measurements were performed with the use of Solver P47-SPM-MDT scanning probe microscope (NT MDT Ltd, Moscow, Russia) in a tapping mode. Images were measured in air at ambient temperature (21 °C) and were stable and reproducible.

TEM images of nanoparticles synthesized in Langmuir monolayer were obtained with the use of JEOL JEM-100B microscope.

3. Results

3.1. Fe-containing nanoparticles

A possible embodiment of the 2-D approach to the synthesis of nanoparticles is the formation of mixed Langmuir monolayer consisted of a volatile metal–organic precursor and surfactant molecules, then photochemical decomposition of the precursor with initiation the 2-D reactions of nanoparticles growth. In a sense, such system represents an ultimately thin photosensitive film. The possibilities for precursor and surfactant molecules to form true monolayer with its diffusion in the plane of monolayer and the structure and homogeneity of the monolayer are important for this approach and are dependent on the surfactant and precursor nature and monolayer compression extent. Thus, amphiphilic properties of precursor and its behavior in the mixed monolayer can be important for the 2-D synthesis method. It was shown previously that iron pentacarbonyl used as a precursor possess amphiphilic properties and can change surface tension of water being deposited on its surface.

The shape of mixed $Fe(CO)_5$/SA monolayer compression isotherm was dependent on the initial $Fe(CO)_5$/SA molar ratio in the monolayer and changed noticeably after UV irradiation and generation of nanoparticles [37]. The compression isotherm shape and quantitative evaluations of the monolayer area per SA molecule in the compressed nanoparticulate monolayer [37] give evidence for the real monolayer structure of resulting nanoparticulate film in which monolayer area per SA molecule only slightly exceeds 20 $Å^2$ what implies that nanoparticles are incorporated in the monolayer in a way when general monolayer structure of surfactant monolayer was not disturbed.

Fig. 1 shows the AFM tapping mode topographic images of a nanoparticulate monolayer deposited onto the surface of mica substrate by the vertical lifting method. Grown nanoparticles are clearly seen in Fig. 1(a) (top view) and 1(c) (3-D image). Nanoparticles were synthesized in a mixed Langmuir monolayer (initial $Fe(CO)_5$/SA ratio was 10:1, UV irradiation 4 min) at $\pi = 0$ (gaseous phase) with low surface concentration of compounds in the monolayer. Fig. 1(b) demonstrates the AFM phase contrast regime image corresponding to the picture 1(a) revealing the difference in material of circular objects and surrounding matrix, thus indicating grown nanoparticles. The AFM image of control monolayer deposited without UV irradiation is shown in Fig. 1(d) giving evidence for rather flat and homogeneous structure of the monolayer without nanoparticles. Fig. 1(e) shows typical height cross-section of the image 1(a) and indicates an overall film roughness of ~ 1 nm with clearly observable nanoparticles of volcano-like morphology with obvious cavity in the central part of nanoparticle. One can see from Fig. 1 that grown nanoparticles are very flatten (height about 1 nm) with very high surface-to-volume ratio (diameter/height ratio ~ 100). The results presented in Fig. 1 show that ultraflattened and even dented nanoparticles with diameters 30–100 nm are formed under the conditions of permanent UV illumination in the rarefied gaseous phase monolayer.

Fig. 2 presents the AFM topographic top view images of the deposited monolayers with nanoparticles synthesized in the compressed mixed monolayer (initial $Fe(CO)_5$/SA ratio was 10:1, UV irradiation 4 min, as in Fig. 1 under surface pressure $\pi \cong 1$ mN m^{-1} (Fig. 2(a)) and under $\pi \cong 2$ mN m^{-1} (Fig. 2(b) and (c)). In this case nanostructures in the monolayers were obtained substantially different in shape and size from those in Fig. 1 with significantly larger diameter (~ 200 nm and more), non-circular shape, but also of extremely small height (~ 1 nm). Fig. 2(c) shows typical height cross-section of the flat nanostructure in Fig. 2(c). Some flat domains possessed ledges of ~ 5 nm height which form aligned aggregates (clearly seen in Fig. 2(b). Quasi-circular nanostructures with tower-like hills were also observed (Fig. 2(a)). The height histogram in Fig. 2(d) clearly demonstrates the terrace structure of the particulate monolayer with main height step about 0.7 nm (diameter/height ratio > 200). The differences observed in morphologies of deposited nanoparticulate monolayers where nanoparticles were synthesized in mixed Langmuir monolayers with the same initial content and under the same UV irradiation conditions but under different monolayer compression extent indicate that kinetic factors (anisotropic 2-D diffusion and surface concentration of reagents and active intermediates) and complex structure of mixed compressed monolayer (also affecting the kinetics of monolayer reactions) play important role in the determination of nanoparticle morphology in 2-D synthesis method.

The AFM images of iron-containing nanoparticles, grown under the same conditions as in Fig. 1 but under external magnetic field (2 kOe) applied parallel to the plane of the monolayer with growing nanoparticles, are shown in Fig. 3 and are different substantially from those in Fig. 1. Shape of nanoparticles in Fig. 3 is close to the oblate semiellipsoid, and characteristic ultraflatten nanoparticles shown in Figs. 1 and 2 were not observed in the sample formed under applied field. One can see aligned prolate nanoparticles in Fig. 3 with aspect ratio about 2 and with rather wide particle size range (nanoparticles smaller than 100 nm, large nanoparticles about 200 nm length and aggregates of some hundred of nanometers in size can be observed). Fig. 3(c)

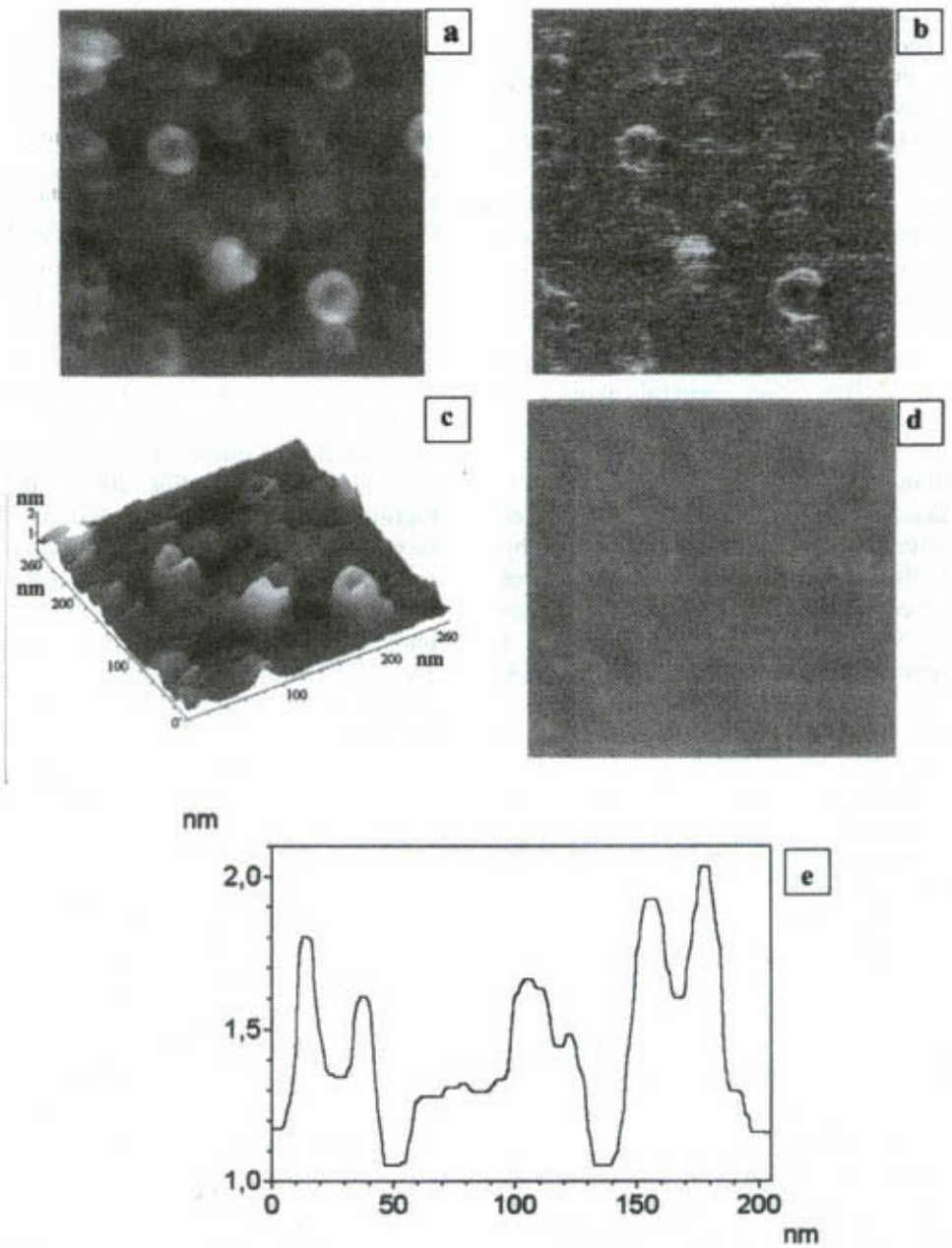

Fig. 1. AFM tapping mode topographic images of iron-containing nanoparticles synthesized in Langmuir monolayer at $\pi = 0$ (initial $Fe(CO)_5$/SA ratio was 10:1, UV exposure time 4 min, $T = 294$ K, sub-phase pH 5.6) and deposited onto the mica substrate at $\pi = 25$ mN m^{-1} using vertical lifting method. Picture (a): AFM topographic image (top view), 280×280 nm^2 scan area, the black-to-white color height scale is 0–2 nm. Picture (b): AFM phase contrast mode top view image corresponding to the image (a). Picture (c): AFM topographic 3-D image corresponding to the image (a). Picture (d): AFM topographic image (top view) of the control monolayer deposited without UV irradiation, 280×280 nm^2 scan area, the black-to-white color height scale is 0–5 nm. (e) Typical height cross-section profile of the image (a).

shows characteristic cross-section profile of the image in Fig. 3(a) indicating that heights of nanoparticles synthesized under applied field parallel to the monolayer plane are at least one order of magnitude larger than the height of particles grown without field. Aligned chain aggregates of nanoparticles were also formed. When external field was applied normal to the plane of the

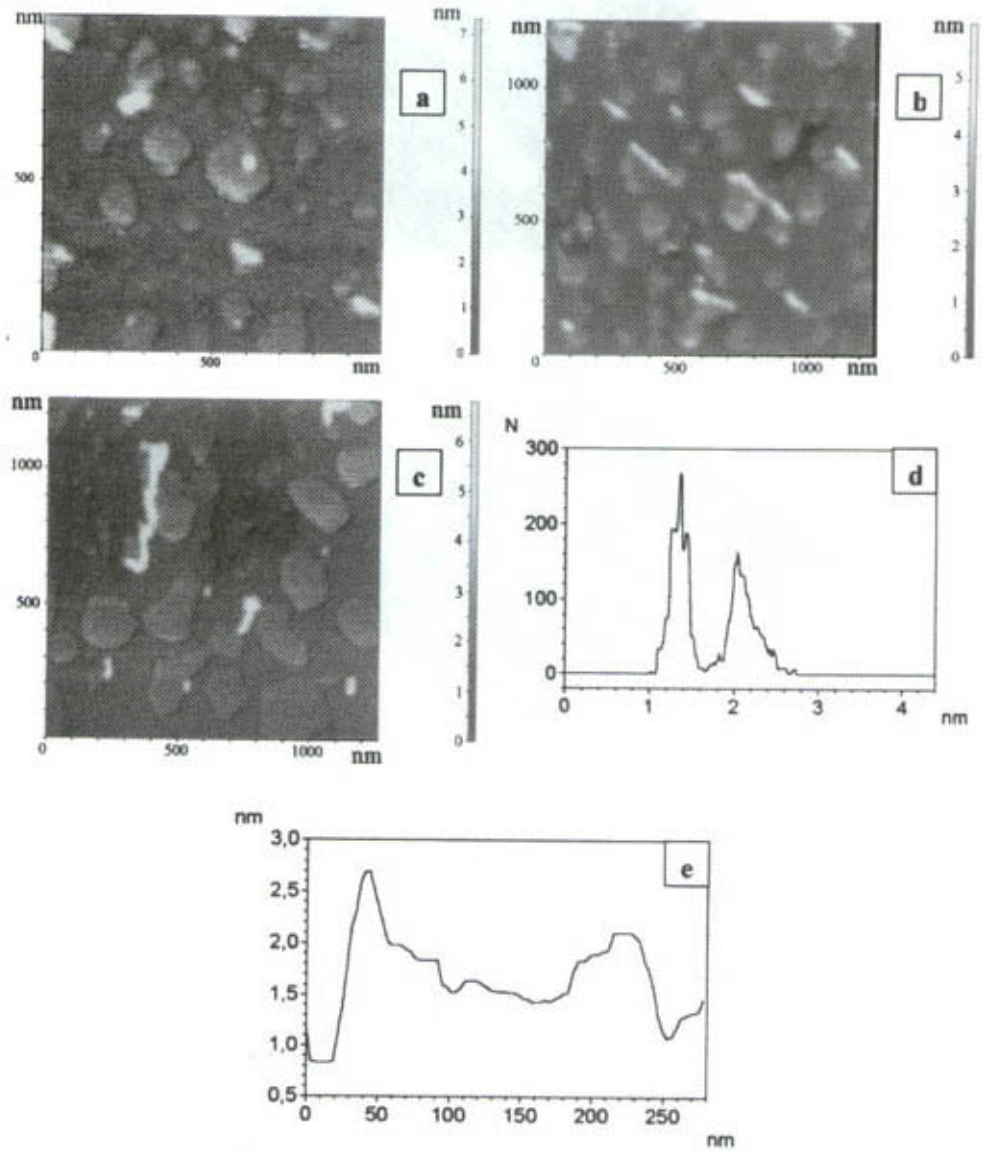

Fig. 2. AFM tapping mode topographic images (top view) of nanostructures synthesized in compressed Langmuir monolayer (initial $Fe(CO)_5$/SA ratio was 10:1, UV exposure time 4 min, $T = 294$ K, sub-phase pH 5.6) and deposited onto the mica substrate at $\pi = 25$ mN m^{-1}. Picture (a): monolayer surface pressure during the synthesis of nanoparticles was $\pi \cong 1$ mN m^{-1}, 1×1 μm^2 scan area, the black-to-white color height scale is 0–7 nm. Picture (b): monolayer surface pressure during the synthesis of nanoparticles was $\pi \cong 2$ mN m^{-1}, 1.2×1.2 μm^2 scan area, the black-to-white color height scale is 0–6 nm. Picture (c): other area of the same sample as in picture (b), 1.2×1.2 μm^2 scan area, the black-to-white color height scale is 0–6.5 nm. Curve (d): height histogram of the image (c). Picture (e): typical height cross-section profile of the flat nanostructure in the image (c) parallel to the x-axis.

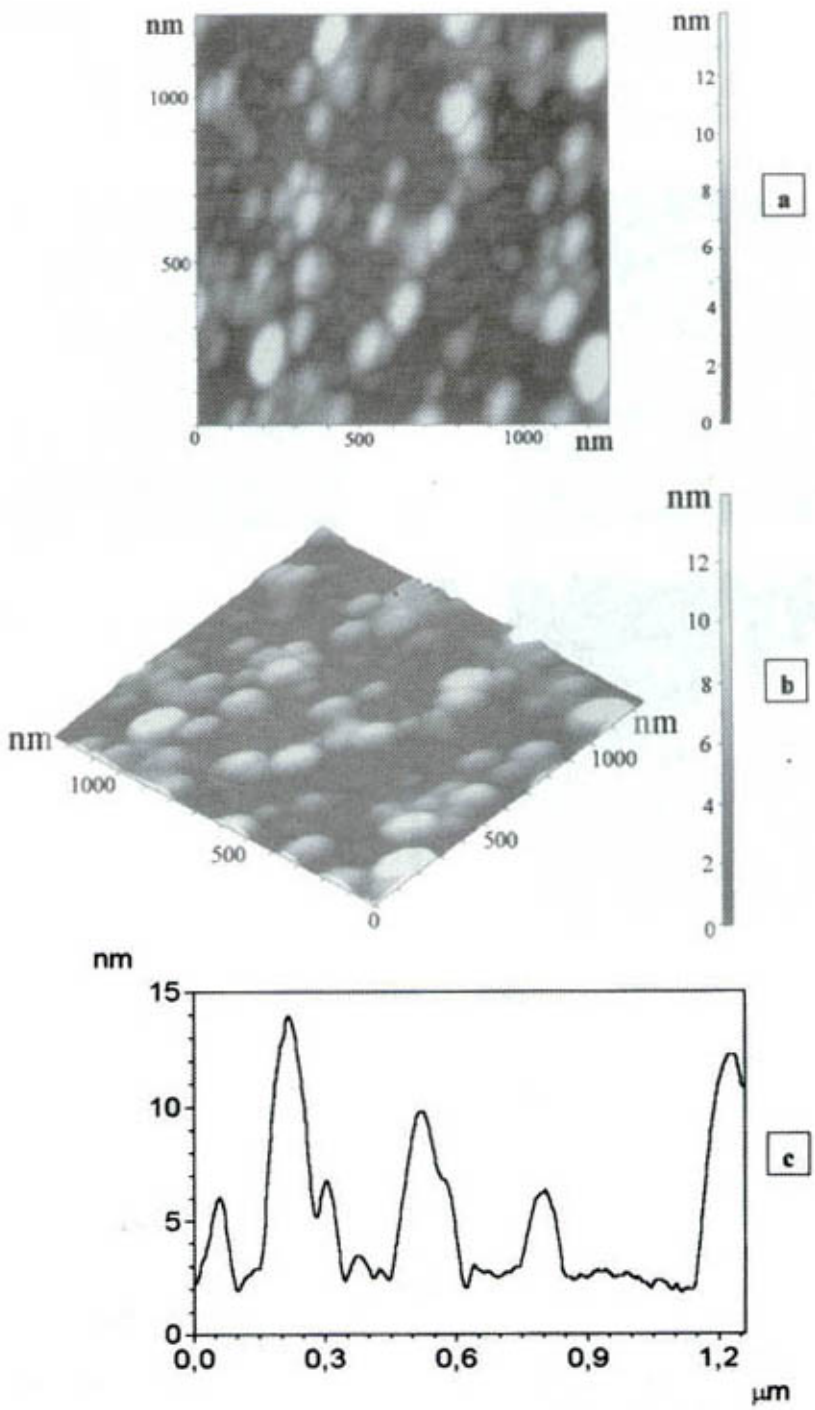

Fig. 3. AFM tapping mode topographic images of iron-containing nanoparticles synthesized in Langmuir monolayer under applied external magnetic field ($H = 2 \times 10^3$ Oe) parallel to the plane of monolayer and deposited under the conditions as in Fig. 1 (initial $Fe(CO)_5$/SA ratio was 10:1, UV exposure time 4 min, $T = 294$ K, sub-phase pH 5.6, monolayer surface pressure during the synthesis of nanoparticles was $\pi = 0$). Picture (a): AFM topographic image (top view), 1.2×1.2 μm^2 scan area, the black-to-white color height scale is 0–14 nm. Picture (b): 3-D AFM topographic image corresponding to the image (a). Picture (c): typical height cross-section profile of the image (a) parallel to the x-axis.

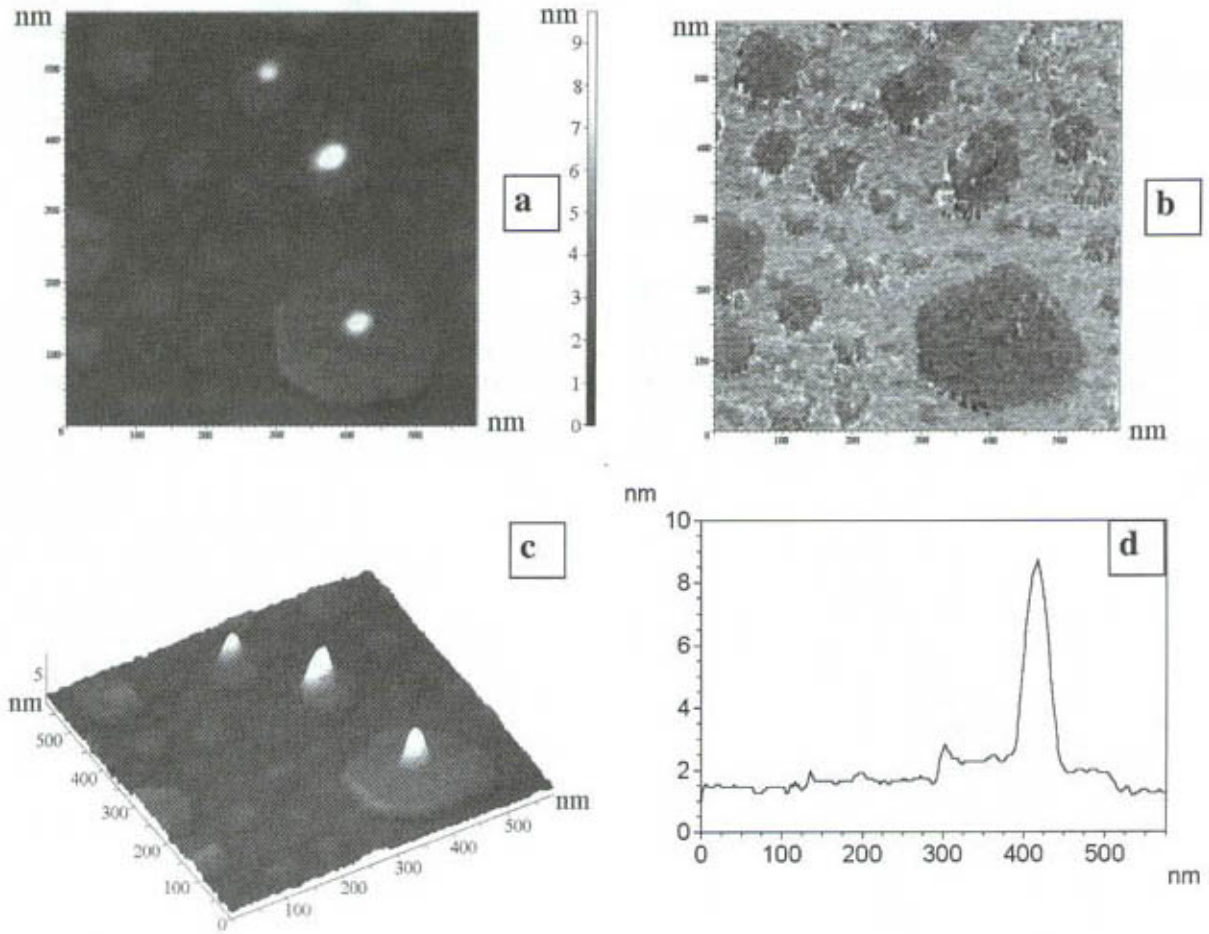

Fig. 4. AFM tapping mode images of nanoparticles synthesized in compressed Langmuir monolayer under applied external magnetic field ($H = 2 \times 10^3$ Oe) perpendicular to the plane of the monolayer (initial $Fe(CO)_5$/SA ratio was 10:1, UV exposure time 4 min, $T = 294$ K, sub-phase pH 5.6, monolayer surface pressure during the synthesis of nanoparticles was $\pi \cong 2$ mN m^{-1},) and deposited to the mica substrate at $\pi = 25$ mN m^{-1}. Picture (a): AFM topographic image (top view), 580×580 nm^2 scan area, the black-to-white color height scale is 0–10 nm. Picture (b): AFM phase contrast mode top view image corresponding to the image (a). Picture (c): 3-D AFM topographic image corresponding to the image (a). Picture (d): typical height cross-section profile of the image (a) parallel to the x-axis.

monolayer with growing nanoparticles, the particles obtained were quasi-circular and of substantially smaller size.

Fig. 4 presents AFM topographic images of nanoparticles synthesized in a mixed compressed monolayer ($\pi = 2$ mN m^{-1}) under applied magnetic field 2 kOe perpendicular to the plane of monolayer. Other conditions were identical to those described in Fig. 3. Fig. 4(b) shows AFM image recorded in a phase contrast regime and corresponding to the images (a) and (c). There is obvious correlation between images indicating the characteristic morphology of the formed nanostructures. Prolate nanoparticles characteristic for uncompressed monolayer under applied field (Fig. 3) were not observed. Besides small flatten quasi-circular nanoparticles with thumbtack-like shape are clearly seen. The nanoparticle of the close

shape was already met in Fig. 2(a) corresponding to the compressed monolayer without applied fields. Fig. 4(d) shows typical results of cross-section analysis of nanoparticulate monolayer shown in Fig. 4(a)–(c) from which characteristic shape parameters of synthesized nanostructures can be derived. Thumbtack-like nanostructures have ~ 0.7 nm thickness flatten foundation and wide peak (~ 7 nm height).

Transmission electron micrography provided more structural information on the formed iron-containing nanoparticles. Figs. 5 and 6 present TEM micrographs showing the nanoparticles and nanostructures obtained with characteristic morphologies. Fig. 5(a) represents the characteristic initial stage of the 2-D formation of large plate-like nanoparticles from small (~ 4 nm) nanoparticles and nuclei under short period of UV illumination (6 s) with immediate compression and deposition of the monolayer. Different characteristic nanoparticle morphologies observed in the experiments described above with 4 min UV illumination corresponding to Figs. 1–4 are presented in Fig. 5 including disks with high (image (c)) and low (image (d)) central area densities, nano-ring (image (e)) and prolate nanoparticle synthesized under applied magnetic field parallel to the plane of the monolayer (image (f)). Fig. 5(b) shows the selected area electron diffraction pattern of the annular region in the nanoparticulate sample corresponding to Fig. 5(a). The absence of visible reflections indicates the amorphous structure of the nanoparticles synthesized. This is consistent with known data when the decomposition of iron pentacarbonyl by ultrasound [42] and thermal treatment [43] leads to the formation of dispersed amorphous iron. Inclusion of other alloying elements is possible and is dependent on reaction conditions and the composition of reaction media [43]. Thus, stable colloidal dispersion of amorphous Fe_2O_3 particles in hexadecane stabilized by oleic acid was produced by sonication of $Fe(CO)_5$ under air conditions [44]. Iron-containing nanoparticles synthesized in the uncompressed Langmuir monolayer formed by $Fe(CO)_5$ without surfactant under 4 min UV illumination are shown in Fig. 6(a). Nanoparticles are characterized by the wide range of the diameter values with main diameter ~ 10 nm. Corresponding selected area electron diffraction pattern is shown in Fig. 6(b) and indicates polycrystalline nature of the sample (with gamma-iron oxide as dominating phase). Fig. 6 represents also the effect of 2-D self-organization and structural evolution in the nanoparticulated SA Langmuir monolayer under the dark incubation after $Fe(CO)_5$ decomposition by short (6 s) UV illumination. Fig. 6(c) and (e) demonstrate the characteristic ramified inorganic nanostructures observed in such deposited monolayer. The nanostructure is composed of quasi-orthogonally organized nanorods with nm-sized clearances in the junctions. Such junctions resemble the skeletal joints and can reflect the mobility of individual nanorods in the nanostructure. Characteristic nanorod is shown in Fig. 6(f). Selected area electron diffraction pattern obtained with nanostructure in Fig. 6(c) is shown in Fig. 6(d). Clear visible point reflexes give evidence for the high degree of crystallinity of the nanostructures formed. Such nanostructures were observed in the mixed monolayers with surfactant while individual nanoparticles and non-ordered aggregates were formed without surfactant under the same reaction conditions. The last observation implies the important role of surfactant molecules in the 2-D self-organization processes of iron-containing magnetic nanoparticles.

3.2. Pd and Au nanoparticles

The other embodiment of the 2-D synthesis method of metallic nanoparticles can be the formation of a mixed monolayer composed of metal–organic precursor and surfactant molecules at the gas/liquid interface with subsequent chemical reduction of the metal to zero-valent state. The formation of noble metal nanoparticles, and, in particular, Pd and Au nanoparticles, in two-phase liquid/liquid system via the reduction of metal-containing precursor compounds in a hydrophobic phase (in particular, in chloroform or toluene) by reducing agents from the aqueous phase (in particular, by sodium borohydride) is known [45–47] and was used to prepare thin nanoparticulate films of palladium using LB tech-

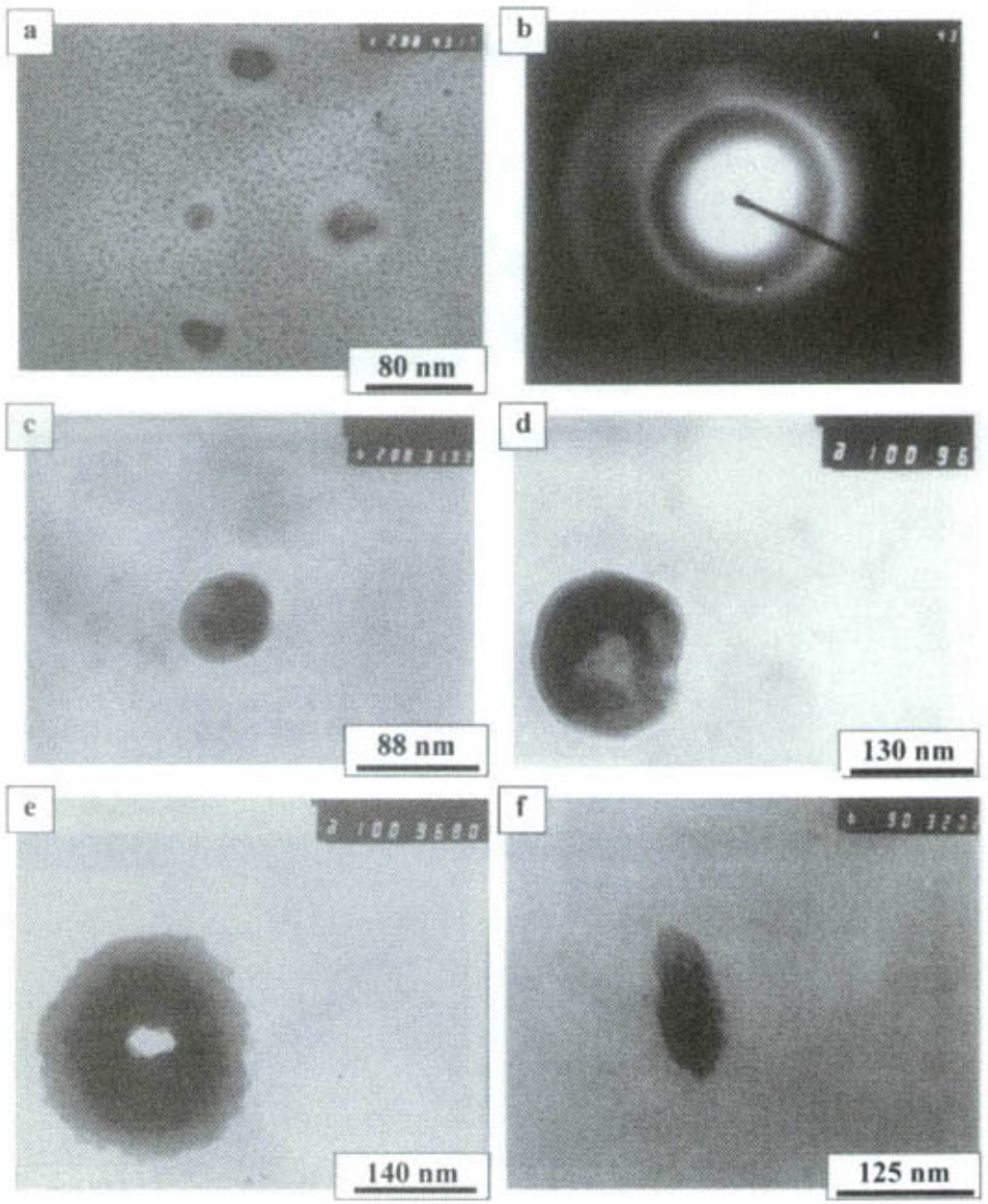

Fig. 5. Transmission electron micrographs showing iron-containing nanoparticles grown in uncompressed Langmuir monolayer and deposited onto the copper grid with Formwar coating at $\pi = 25$ mN m^{-1}. Conditions for nanoparticle synthesis for the image (a): initial $Fe(CO)_5$/SA ratio 10:1, UV exposure time 6 s, $T = 294$ K, sub-phase pH 5.6, monolayer surface pressure during the synthesis of nanoparticles $\pi = 0$. Conditions for nanoparticle synthesis for images (d) and (e) were the same as in Fig. 1; conditions for nanoparticle synthesis for image (c) were the same as in Fig. 4. Conditions for nanoparticle synthesis for image (f) were the same as in Fig. 3. Image (b)—typical selected area electron diffractogram obtained from the samples with iron-containing nanoparticles.

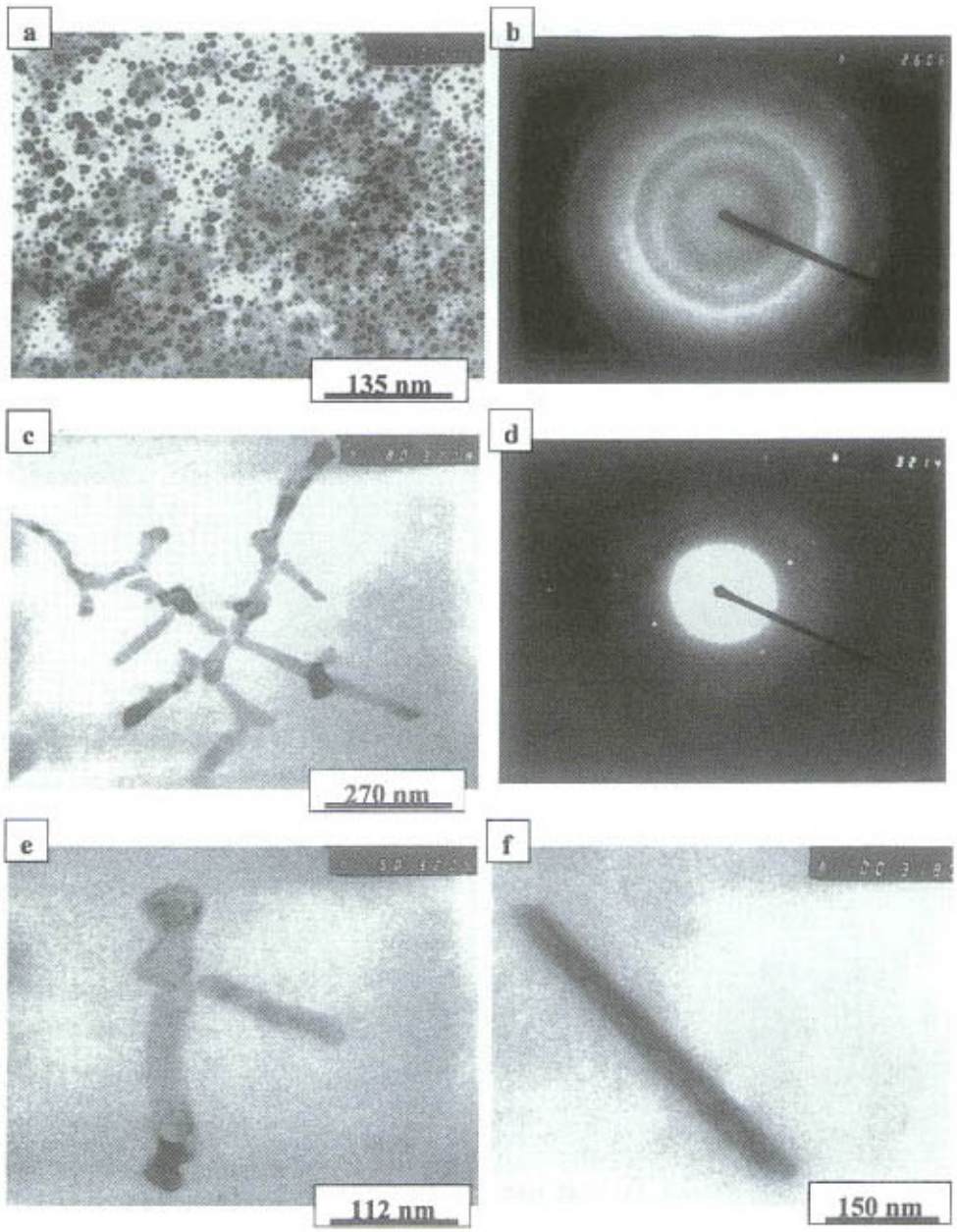

Fig. 6. Transmission electron micrographs showing iron-containing nanoparticles and nanostructures grown in uncompressed Langmuir monolayer and deposited onto the copper grid with Formwar coating at $\pi = 25$ mN m^{-1}. Image (a): monolayer was formed by $Fe(CO)_5$ without surfactant, UV exposure time 4 min, $T = 294$ K, sub-phase pH 5.6, monolayer surface pressure during the synthesis of nanoparticles $\pi = 0$. Reaction conditions for images (c)–(e) were: initial $Fe(CO)_5$/SA ratio 5:1, UV exposure time 6 s, dark incubation of the monolayer after UV illumination 4 min, $T = 294$ K, sub-phase pH 5.6, monolayer surface pressure during the UV illumination and following dark incubation $\pi = 0$. Image (b): selected area electron diffractogram obtained from the sample with iron-containing nanoparticles shown in (a); image (d): selected area electron diffractogram obtained with nanostructure shown in (c).

nique [48]. To demonstrate the possibilities of the 2-D synthesis approach to control the shape of noble metal nanoparticles the $Pd_3(CH_3COO)_6$ and $Au(P(C_6H_5)_3)Cl$ molecules were used as a water-insoluble precursors in the present work. In this embodiment the reduction of noble metal to zero-valent state in a mixed precursor plus surfactant Langmuir monolayer floating on the surface of the aqueous sub-phase containing sodium borohydride can be considered as an ultimate version of a two-phase reducing system in which precursor phase represents an ultimately thin monomolecular structure. Mixed LB films of fatty acids and different metal–organic nanocluster and complex molecules with structure and properties close to the precursors used in the present work were studied previously in our group and it was shown by the scanning tunneling microscopy technique with sub-molecular resolution that such mixed supramolecular systems can be true monolayers [49].

Fig. 7 represents the AFM tapping mode topographic images of Pd nanoparticles synthesized at the gas/sodium borohydride aqueous solution interface without surfactant at low surface density of $Pd_3(CH_3COO)_6$ molecules at $\pi = 0$, and deposited onto the mica substrate at $\pi = 18$ mN m^{-1}. Fig. 7(a) and (b) demonstrate characteristic topographies observed in the sample. It can be seen that many particles have coalesced to form complex supraparticulate structures. Areas with regular 3-D aggregates of quasi-spherical nanoparticles were found with mean nanoparticle size ~ 30 nm. Fig. 7(c) demonstrates an enlarged image of such a 'crystal of nanoparticles'. At the same time areas with rather planar arrays of quasi-spherical nanoparticles were observed (Fig. 7(b) and (d)). Height cross-section profile of nanoparticulate aggregate from Fig. 7(c) is present in Fig. 7(e) and height cross-section of image (d) parallel to the x-axis is shown in Fig. 7(f) demonstrating the pronounced 3-D character of morphologies of the nanostructures synthesized.

Superstructures firmed by Pd nanoparticles synthesized at the gas/sodium borohydride solution interface without surfactant but under the surface pressure value $\pi \cong 1$ mN m^{-1} are shown in Fig. 8. In this case macroscopic aggregates of nanoparticles with two characteristic morphologies were formed. One is shown in Fig. 8(a) and (c), and represents rather irregularly aggregated large nanoparticles (~ 200 nm). The other is a system of aligned quasi-parallel strings of nanoparticles (nanoparticle size was also about 200 nm). Macroscopic string-like structures can be a result of anisotropy of interparticle interactions on the aqueous phase surface introduced by slight planar compression of the interface area.

It is known that the presence of surfactant during the formation of metal nanoparticles can influence the resulted nanoparticle morphology [27,48,50]. Fig. 9 shows typical AFM tapping mode topographic images of Pd nanoparticles synthesized in a mixed Langmuir monolayer with arachidic acid ($Pd_3(CH_3COO)_6$/AA ratio was 1:1) at the gas/aqueous sodium borohydride solution interface at $\pi = 0$. One can see from Fig. 9 that the presence of surfactant changes substantially the morphology of grown nanoparticles and of deposited particulate monolayer as a whole. Images 9(a) and (b) represent characteristic aggregates of nanoparticles observed in the deposited monolayer. Aggregates are of quasi-chain (Fig. 9(a) and (c)) and of plate-like and complex planar character (Fig. 9(b) and (d)) should determined by the attractive interparticle van der Waals interaction (dependent on the particle size) and by surfactant effects. AFM phase contrast mode top view image corresponding to Fig. 9(c) is shown in Fig. 9(e) and supports the presence of nanoparticles in the monolayer. Nanoparticles are ~ 50 nm in diameter as clearly seen from Fig. 9(c), (d) and (f). Important feature is that nanoparticles are of pronounced oblate character (about 5 nm height).

The nature of surfactant forming the organic template where metal nanoparticles are generated often influence shape and size of the grown nanoparticles [33]. Fig. 10 demonstrates the effect of surfactant nature on the morphology of Pd nanostructures formed by the 2-D synthesis method. Instead of arachidic acid octadecyl amine was used as a surfactant to form mixed Langmuir monolayer with $Pd_3(CH_3COO)_6$–ODA ratio 1:1. The other conditions for Pd nanoparticles growth were the same as in Fig. 9, but the shape of the

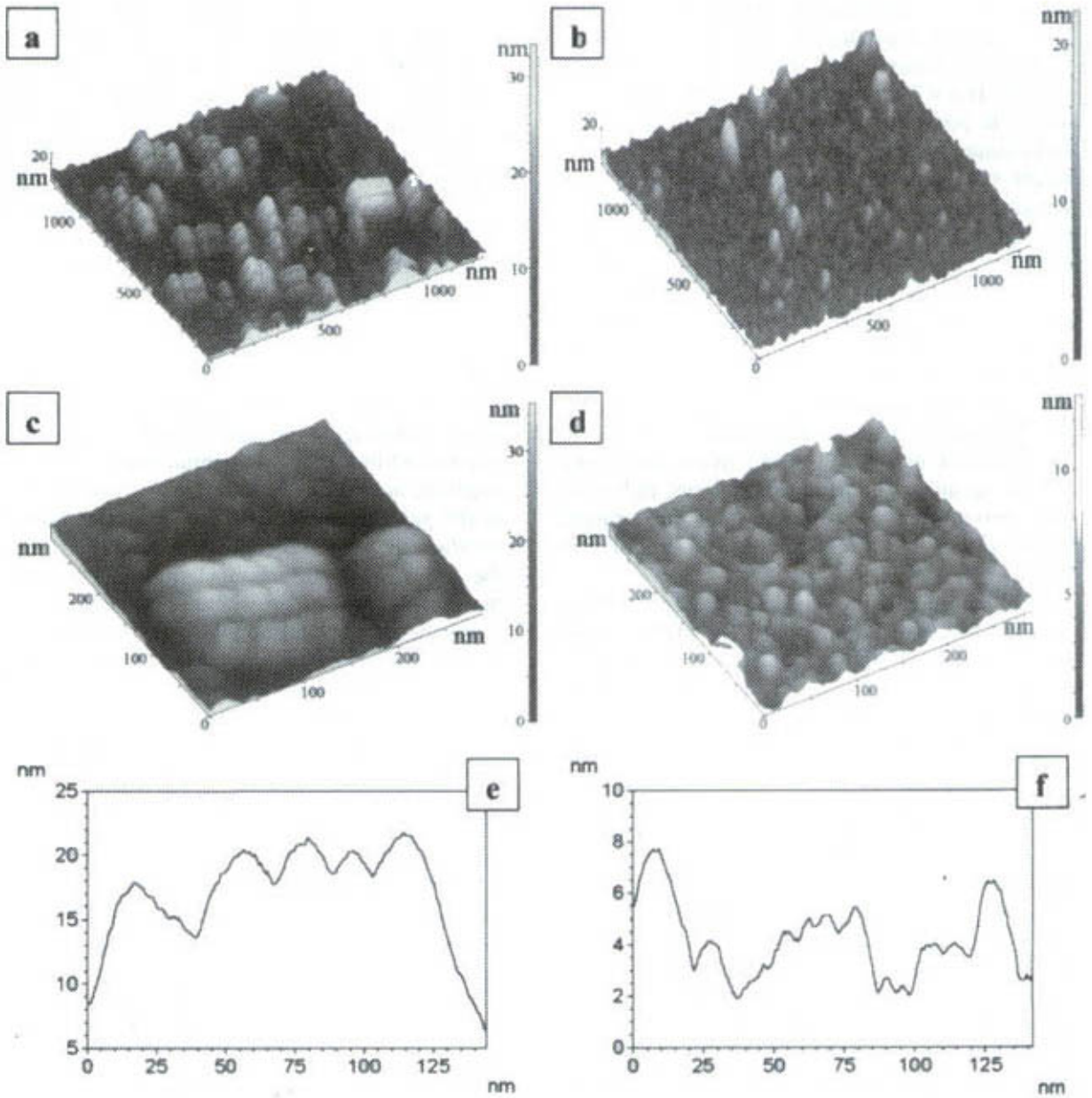

Fig. 7. AFM tapping mode topographic images of Pd nanoparticles synthesized at the gas/sodium borohydride solution interface without surfactant at $\pi = 0$ and deposited onto the mica substrate at $\pi = 18$ mN m^{-1}. Spreading solution of $Pd_3(CH_3COO)_6$ in chloroform (10^{-4} M) was used, $T = 294$ K, aqueous sub-phase contained 5×10^{-3} M $NaBH_4$. Picture (a): AFM topographic 3-D image, 12.5×12.5 μm^2 scan area, the black-to-white color height scale is 0–36 nm. Picture (b): AFM topographic 3-D image, 12.5×12.5 μm^2 scan area, the black-to-white color height scale is 0–22 nm. Picture (c): enlarged view of the part of the area with 3-D aggregate shown in (a), 280×280 nm^2 scan area, the black-to-white color height scale is 0–36 nm. Picture (d): enlarged view of a part of the area shown in (b), 280×280 nm^2 scan area, the black-to-white color height scale is 0–13 nm. Curve (e): height cross-section profile of the aggregate shown in the image (c). Curve (f): typical height cross-section profile of image (d) parallel to the x-axis.

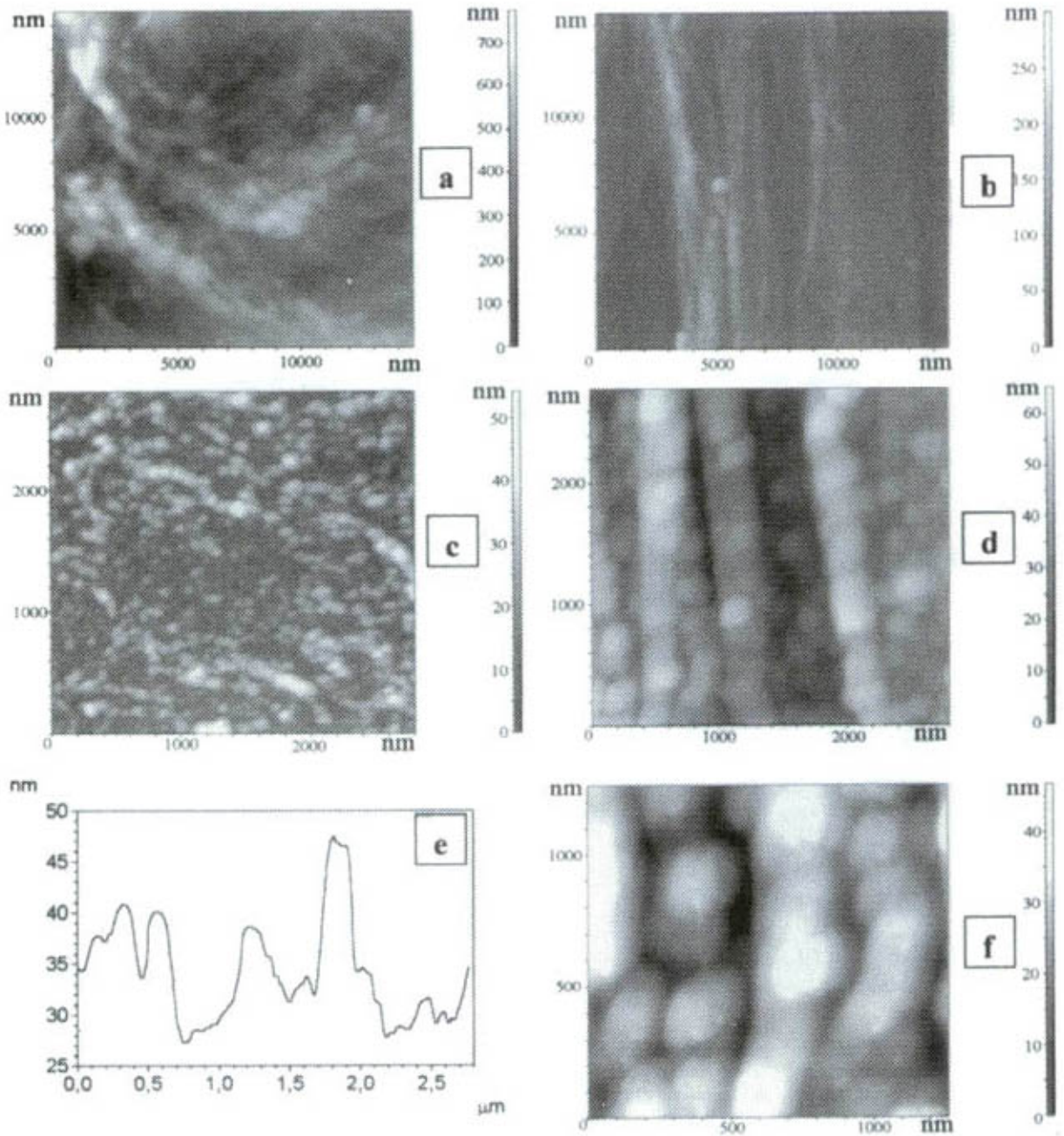

Fig. 8. AFM tapping mode topographic top view images of Pd nanoparticles synthesized at the gas/sodium borohydride solution interface without surfactant at $\pi \cong 1$ mN m^{-1} and deposited onto the mica substrate at $\pi = 18$ mN m^{-1}. Spreading solution of $Pd_3(CH_3COO)_6$ in chloroform (10^{-4} M) was used, $T = 294$ K, aqueous sub-phase contained 5×10^{-3} M $NaBH_4$. Picture (a): AFM topographic image, 14.5×14.5 μm^2 scan area, the black-to-white color height scale is 0–760 nm. Picture (b): AFM topographic image, 14.5×14.5 μm^2 scan area, the black-to-white color height scale is 0–300 nm. Picture (c): enlarged view of one part of the area shown in Fig. 7(a), 2.8×2.8 μm^2 scan area, the black-to-white color height scale is 0–60 nm. Picture (d): enlarged view of the part of the area shown in (b). 2.8×2.8 μm^2 scan area, the black-to-white color height scale is 0–65 nm. Curve (e): typical height cross-section profile of the image (d) along the y-axis. Picture (f): enlarged view of the part of the area shown in (d) 1.25×1.25 μm^2 scan area, the black-to-white color height scale is 0–46 nm.

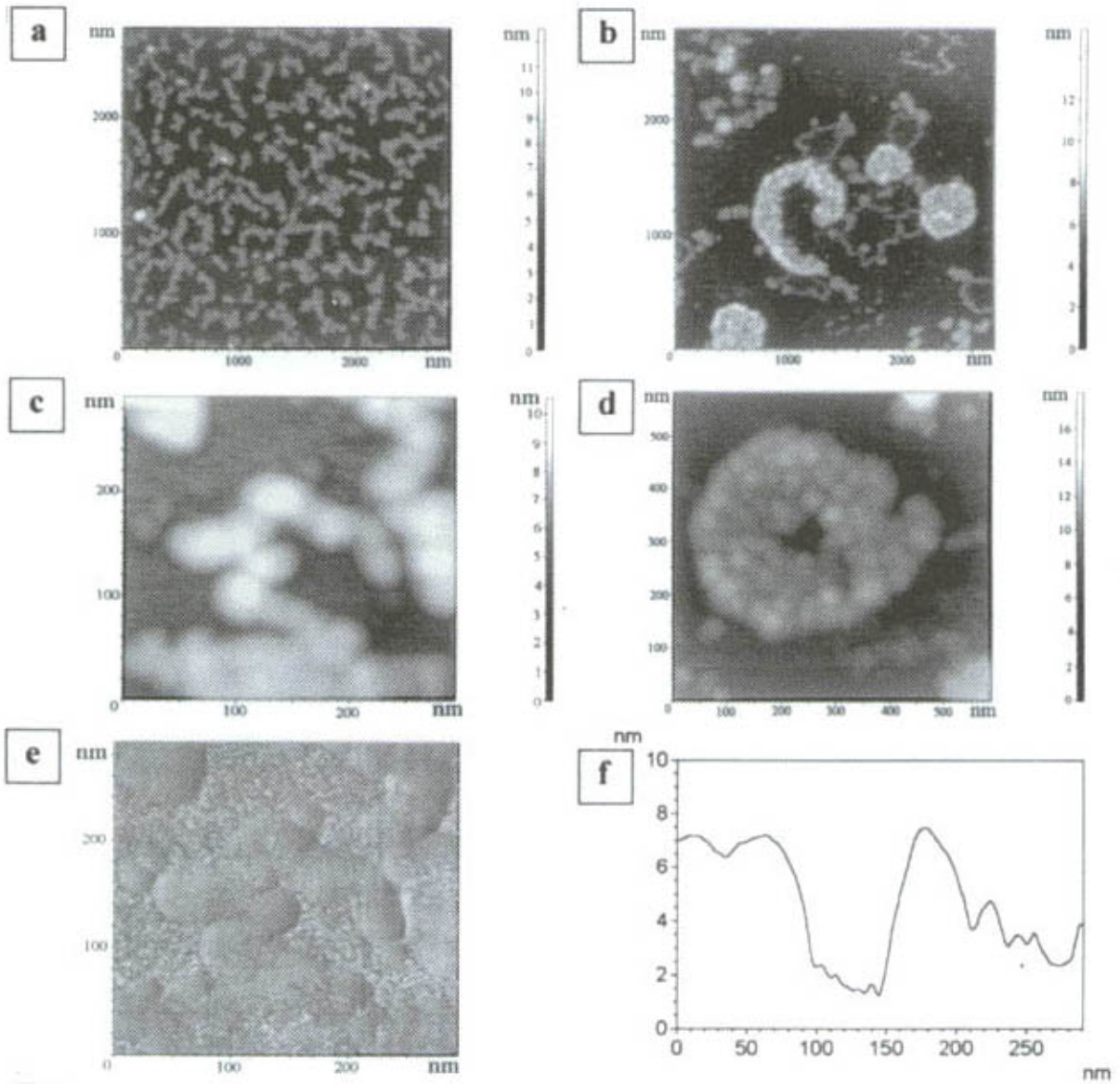

Fig. 9. AFM tapping mode topographic images of Pd nanoparticles synthesized in Langmuir monolayer at the gas/sodium borohydride solution interface at $\pi = 0$ and deposited onto the mica substrate at $\pi = 25$ mN m^{-1}. Spreading solution of $Pd_3(CH_3COO)_6$/AA with 1:1 ratio in chloroform (10^{-4} M AA) was used, $T = 294$ K, aqueous sub-phase contained 5×10^{-3} M $NaBH_4$. Picture (a): top view image, 2.8×2.8 μm^2 scan area, the black-to-white color height scale is 0–12 nm. Picture (b): top view image, 2.8×2.8 μm^2 scan area, the black-to-white color height scale is 0–14 nm. Picture (c): enlarged view of a part of the area shown in (a), 290×290 nm^2 scan area, the black-to-white color height scale is 0–10.5 nm. Picture (d): enlarged view of a part of the area of the sample shown in (b), 680×680 nm^2 scan area, the black-to-white color height scale is 0–16 nm. Picture (e): AFM phase contrast mode top view image corresponding to the image (c). Curve (f): typical height cross-section profile of the image (c) parallel to the x-axis.

nanoparticles obtained was substantially different. One can see that nanostructures (possibly aggregates of very fine nanoparticles) in Fig. 10 are substantially more flatten with mean height ~1.3 nm (and diameter up to 100 nm). The homogeneous flatten morphology of these nanostructures is clearly illustrated in Fig. 10(c) where height histogram of image (a) is presented with two broad peaks corresponding to most frequently present structure heights with main height difference about 1.3 nm demonstrating the terrace structure of the particulate monolayer with main height step about 1.3 nm. Important point is that Pd nanoparticles with characteristic thumbtack-like shape were present in this sample. Iron-containing nanoparticles with analogous shape were demonstrated in Figs. 2(a) and 4.

Results of TEM investigations of the Pd particulate films transferred to the copper grid with Formwar coating are shown in Fig. 11. The TEM micrographs obtained from nanoparticulate samples formed without surfactant (images (a) and (b)) under conditions as in Fig. 8 are in good agreement with AFM data presented in Figs. 8 and 11(c),(e) illustrate the effect of initial $Pd_3(CH_3COO)_6$/AA ratio in the mixed monolayer on the morphology of resulted Pd nanoparticles. High $Pd_3(CH_3COO)_6$/AA ratio 5:1 (Fig. 11(c))

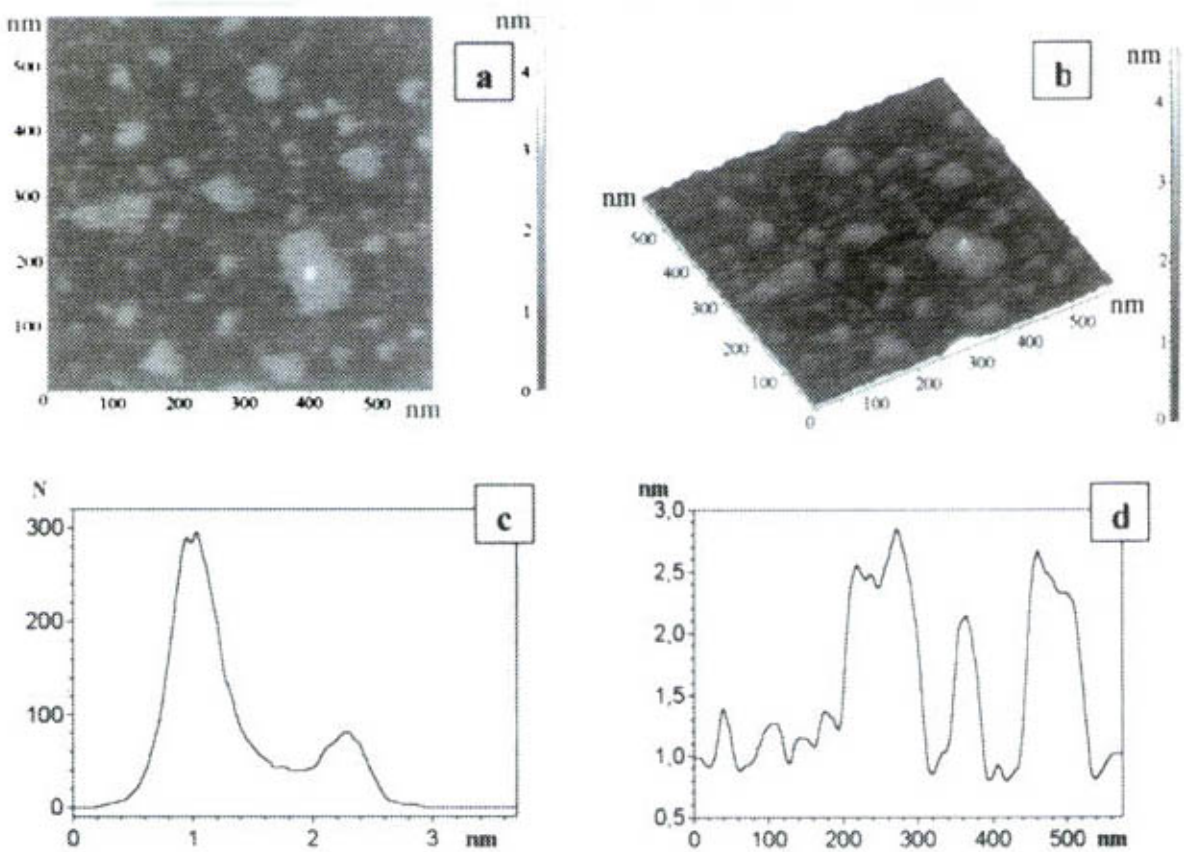

Fig. 10. AFM tapping mode topographic images of Pd nanoparticles synthesized in Langmuir monolayer at the gas/sodium borohydride solution interface at $\pi = 0$ and deposited onto the mica substrate at $\pi = 25$ mN m^{-1}. Spreading solution of $Pd_3(CH_3COO)_6$/ODA with 1:1 ratio in chloroform (10^{-4} M ODA) was used, $T = 294$ K, aqueous sub-phase contained 5×10^{-3} M $NaBH_4$. Picture (a): top view image, 580 × 580 nm^2 scan area, the black-to-white color height scale is 0–4.6 nm. Picture (b): AFM topographic 3-D image corresponding to the image 10(a). Curve (c): height histogram of the image (a). Curve (d): typical height cross-section profile of the image 10(a) parallel to the x-axis.

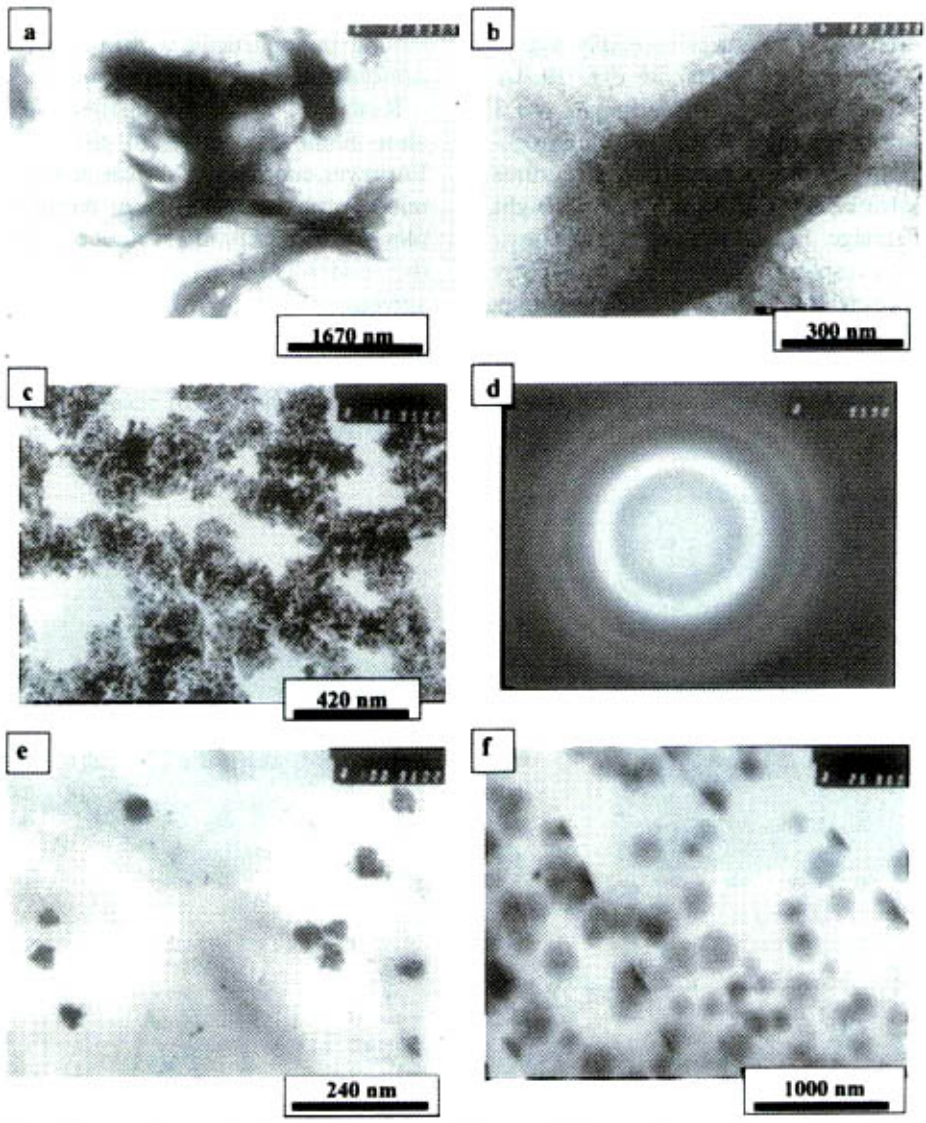

Fig. 11. Transmission electron micrographs showing Pd nanoparticles grown in Langmuir monolayer and deposited onto the copper grid with Formwar coating. Conditions for nanoparticle synthesis for images (a) and (b) were the same as in Fig. 8, conditions for nanoparticle synthesis for the image (c) were: $Pd_3(CH_3COO)_6$/AA ratio = 5:1, aqueous sub-phase contained 5×10^{-3} M $NaBH_4$. Conditions for nanoparticle synthesis for images (e) and (f) were the same as in Figs. 9 and 10, correspondingly. Image (d): selected area electron diffraction pattern obtained for nanoparticles shown indicating polycrystalline Pd.

leads to the formation of nanoparticle aggregates with structure resembling those observed for the bulk phase solution reduction of palladium salts [51]. The TEM micrographs Fig. 11(e) and (f) obtained with samples prepared under the same conditions as in Figs. 9 and 10, correspondingly, are not characteristic for nanoparticles grown by the bulk-phase techniques and reveal the particular morphological features of nanostructures formed by the 2-D synthesis method. Characteristic selected area electron diffraction pattern obtained for Pd nanoparticles is shown in Fig. 11(d) indicating polycrystalline metallic Pd.

The results of TEM analysis of gold nanoparticles synthesized in Langmuir monolayer using 2-D synthesis approach are presented in Fig. 12. Fig. 12(a) shows the control sample with Au nanoparticles synthesized at the gas/sodium borohydride aqueous solution interface without surfactant at low surface density of $Au(P(C_6H_5)_3)Cl$ molecules at $\pi = 0$ and deposited onto the TEM substrate at $\pi = 18$ mN m^{-1}. Fig. 12(b) shows characteristic TEM image of Au nanoparticles synthesized in a mixed Langmuir monolayer (initial $Au(P(C_6H_5)_3)Cl$–ODA ratio was 1:5) onto the aqueous sodium borohydride solution sub-phase at $\pi = 0$. The effect of 2-D self-organization of Au nanoparticles with formation of complex anisotropic nanostructure under incubation of a particulate ODA monolayer is illustrated by Fig. 12(c). Characteristic selected area electron diffraction pattern presented in Fig. 12(d) indicates polycrystalline metallic Au in the samples studied. Pictures 12(e) and (f) show size distribution histograms of Au nanoparticles corresponding to the images 12(a) and (b), respectively. It follows from the pictures that Au nanoparticles synthesized in a mixed surfactant monolayer are characterized by smaller size (main diameter ~ 1.5 nm) and narrower size distribution in comparison with Au nanoparticles formed without surfactant.

4. Discussion

The experimental data presented in Figs. 1–12 illustrate the possibilities of 2-D synthesis approach to obtain anisotropic nanoparticles and nanostructures with metals of substantially different nature and with controllably variable unique morphologies. In fact, such approach could open new possibilities for insight into the fine mechanisms of nanoscale processes. Effects of nucleation, growth, interparticle interactions, self-organization and structure formation can be examined experimentally from the new point in this approach, giving stimulus for theoretical modeling. It seems hardly at the moment to give detail explanation of all 2-D reactions and effects resulted in the observed characteristic morphologies of grown nanoparticles and nanostructures, future investigations will elucidate it. However, it seems appropriately to discuss some major points.

The principal feature of the 2-D synthesis approach which distinguishes it from the other methods of nanoparticle synthesis is the formation of dynamic 2-D reaction system—a true monolayer at the gas/liquid interface formed by metal–organic precursors and surfactant molecules, which is reaction area of exactly 2-D character. Decomposition of an insoluble metal–organic precursor compound in a mixed surfactant monolayer at the gas/liquid interface and resulting growth of nanoparticles are examples of 2-D processes where true 2-D diffusion of precursor molecules, active intermediates, metal atoms and its complexes, nucleus and nanoparticles, surfactants and additives occurs only in the monolayer at the gas/liquid interface allowing them to move and interact only in the plain of monolayer. It is known that the phase and structural state of Langmuir monolayers (in particular, fatty acid monolayers) can be changed under compression from 2-D gas to 2-D condensed phases via phase transitions [39], and potentially 2-D synthesis of nanoparticles can be carried out in a monolayer under different compression states. In compressed monolayers structural heterogeneities can exist as domains of coexisting phases or of different compounds present in the monolayer. Structurally homogeneous state of a mixed monolayer generally can be gaseous and liquid phases where molecules are free to diffuse in the plane of a monolayer, and high degree of mixing can be achieved. Besides, surface concentrations of monolayer compounds can be widely regulated in these phases. Such approach allows to form rarefied 2-D gas-like systems of precursor molecules. Figs. 1 and 2 demonstrate effects of variations in the monolayer compression extent on the morphology of the grown nanoparticles. Thus, the compression of a mixed monolayer can be an instrument for the control of nanoparticles formation in the 2-D synthesis method.

The general feature of nanoparticles synthesized in a monolayer at the gas/liquid interface is its substantially flatten shape (down to a few atoms thickness) when the growth process was carried out in a mixed surfactant Langmuir monolayer

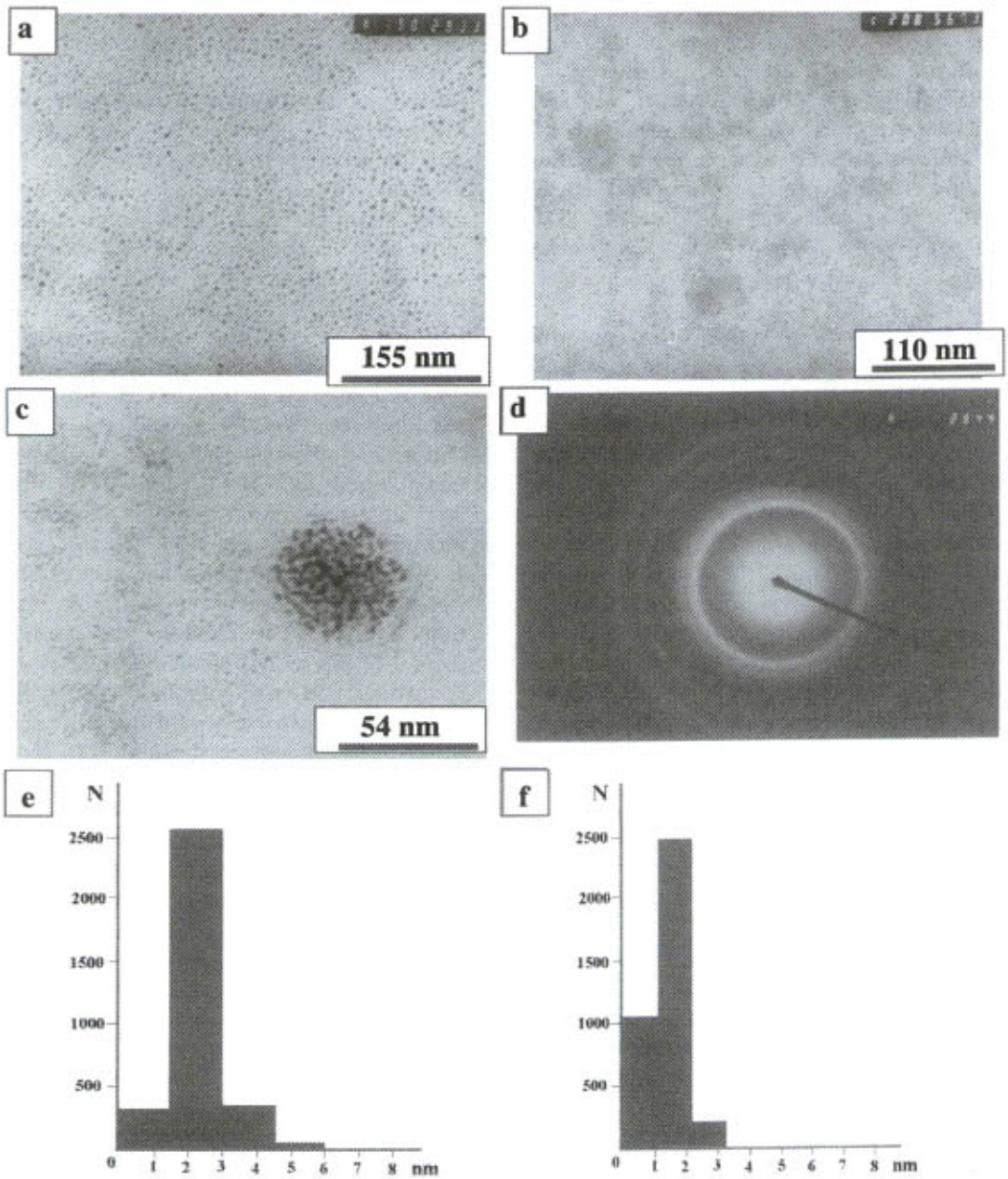

Fig. 12. Transmission electron micrographs showing Au nanoparticles grown in Langmuir monolayer and deposited onto the copper grid with Formwar coating. Image (a): control sample with Au nanoparticles synthesized at the gas/sodium borohydride aqueous solution interface without surfactant at low surface density of $Au(P(C_6H_5)_3)Cl$ molecules at $\pi = 0$ and deposited onto the TEM substrate at $\pi = 18$ mN m^{-1}. Spreading solution of $Au(P(C_6H_5)_3)Cl$ in chloroform (10^{-4} M) was used, $T = 294$ K, aqueous sub-phase contained 5×10^{-3} M $NaBH_4$. Images (b) and (c): Au nanoparticles synthesized in a mixed Langmuir monolayer (initial $Au(P(C_6H_5)_3)Cl$/ODA ratio 1:5) onto the aqueous sodium borohydride solution (5×10^{-3} M $NaBH_4$) at $\pi = 0$; monolayer corresponding to the image (c) was additionally incubated for 20 min. Image (d): characteristic selected area electron diffraction pattern observed for the particulated samples presented in Fig. 12. Images (e) and (f): size distribution histograms of Au nanoparticles corresponding to the images (a) and (b), respectively.

independently on the synthesis routine and metal nature. However, without surfactant rather 3-D nanoparticles were formed (Figs. 7 and 8). Two-dimensional synthesis method allows also to form suprananoparticulate structures—ordered aggregates shown in Figs. 6(c), (e), 7(a), (c), 8(b), (d) and 12(c). These observations give evidence for the important role of surfactant in the 2-D synthesis method to direct the nanoparticle growth into an anisotropic planar way. Possibly, long hydrocarbon chains in molecules of surfactants being localized in a plane of uncompressed monolayer with its polar groups interacting with metallic nucleus and nanoparticles can fix effectively its orientation and hinder its rotation relatively to the axis deviated from the normal to the monolayer. In this connection the noticeable difference in the shape of Pd nanoparticles synthesized with octadecyl amine and arachidic acid (in the last case nanoparticles were more bulky) can be due to the differences in the affinity of these surfactants to Pd.

The detailed mechanism of nanoparticle growth in a monolayer at the gas/liquid interface is still not known at this stage; however, evidences suggest that the role of anisotropic geometric factors, surfactant interactions with intermediates, nuclei and nanoparticles, and monolayer structure may be important for 2-D space distribution and diffusion control of all components, and also for restriction of rotation and aggregation of nanoparticles. The effects of temperature on these processes can result in shape modifications of two-dimensionally grown nanoparticles. Also, kinetics of 2-D growth is dependent on the surface concentration and the rate of decomposition of precursors. It is known that the crystal structure of metal particulates is dependent on the reduction rate, and particulates formed under conditions of fast reduction are usually smaller in size [52]. Two-dimensional synthesis approach allows to control effectively the nanoparticle growth rate via the distribution of precursor molecules in the plane of a monolayer and its mixing with surfactants and additives along with the varying of the rate of precursor decomposition and generation of active intermediates and metal atoms. Thus, the variation in UV illumination conditions (and, in particular, flash regime) allows changing the morphology of nanoparticles grown photochemically via iron pentacarbonyl decomposition due to kinetic factors and yields amorphous and crystalline nanoparticles and nanostructures (Figs. 5 and 6).

The formation of oblate metallic nanoparticles in layered organic matrix was reported in literature. Thus, relatively thick metallic gold nanoparticles were photochemically generated in multilayer LB films of positively charged amphiphiles deposited from the aqueous $HAuCl_4$ sub-phase (diameter of nanoparticles ranged from 20 to 800 nm and height was 15–20 nm, lamellar structure of LB films was disrupted after the particles formation) [33]. It was concluded that the oblate shape of grown nanoparticles was essentially connected with quasi-2-D character of the growth processes and diffusion of intermediates parallel to the planes of surfactant layers in LB film.

Metallic particles usually aggregate under contact (it is clearly seen from Figs. 7 and 8) and it is necessary to stabilize nanophase materials. Surface active compounds are usually used for this purpose. In the 2-D synthesis approach surfactants play a double role—to passivate and stabilize growing nanoparticles and to form monolayer at the gas/liquid interface. It is clear from comparison of Pd nanoparticles in Figs. 9 and 10 that the morphology of resulting nanoparticles is dependent on the nature of surfactant used. The effect of surfactant type on the morphology of gold nanoparticles grown in multilayer LB films was also observed in Ref. [33]. Thus, the type of surfactant and/or additive present in a mixed monolayer (or a number of different surfactants present simultaneously) can be the other instrument for the shape control of nanoparticles in the 2-D synthesis method. Special effects of amphiphilic polymers and oligomers on the morphology of two-dimensionally grown nanostructures can be expected along with effects of liquid phase compounds interacting with monolayer.

There is characteristic thumbtack-like shape of the nanoparticles obtained observed for iron-containing photochemically generated particles and Pd particles grown via chemical reduction (Figs. 2, 4 and 10). Such metal nature and synthetic

route independent shape can be a result of specific 2-D kinetic effects when the rate of nanoparticle growth at first stage is higher (possibly, due to high initial local surface concentration of precursor) than at later stages what leads to fast quasi-3-D growth at the first stage and rather slow 2-D growth in subsequent stages. There are data in literature on the formation of flatten semiconductor CdS nanoclusters in LB films that the slowing down of 2-D nanoparticle growth rate results in the formation of more flatten nanoparticles [35,53].

Figs. 3 and 5(f) demonstrate the effect of external applied field on the shape of grown iron-containing nanoparticles. These AFM and TEM results are in good agreement with STM data earlier obtained in our group on the effects of applied fields on the morphology of magnetic nanoparticles [54] and with literature data [55]. Magnetic properties of particulate multilayer LB films with iron-containing nanoparticles formed by the 2-D synthesis method were studied using electron paramagnetic resonance technique [54]. The ferromagnetic resonance and superparamagnetic signals were observed in the material, indicating magnetic moments of the grown particles [54]. STM analysis of the deposited nanoparticulate monolayers showed that morphology of magnetic nanoparticles formed at the gas/water interface via decomposition of iron pentacarbonyl was changed substantially when external magnetic field was applied during the synthesis. It was found that the size and shape of nanoparticles were strongly dependent on the applied field orientation relatively to the monolayer surface. It is well-known that metallic and metal-containing nanoparticles can posses magnetic dipolar moment and also an electric dipolar moment due to the conducting particle polarization under external electric field. Anisotropic interparticle dipole–dipole interactions in colloid systems under applied fields are used in electrorheological fluids [56] and ferrofluids [40]. Effects of synergistically applied electric and magnetic fields to enhance the interactions of colloid magnetic conducting particles were exploited in magnetoelectrorheological liquids [57,58]. It was concluded that anisotropic interparticle dipole–dipole interactions and kinetic factors can play important role in the dipolar nanoparticle growth reactions under applied external fields [54,59]. As a result, applied external fields could be an instrument for controlling the growth processes and morphology of nanoparticles and nanostructures in the 2-D synthesis method.

Interesting type of nanostructure shape—nanoring was specifically observed for magnetic iron-containing nanoparticles (Figs. 1 and 5(e)) and not for Pd or Au nanoparticles. Such structures were obtained only without applied magnetic field and under conditions of permanent UV illumination. Ring shape can be a result of the 2-D self-organization of growing nanoparticles in the plane of a monolayer due to the magnetic dipolar interactions and formation of coalesced ring aggregates. Such scenario correlates with theoretical results of Ref. [60] where formation of circular aggregates of magnetic colloids and its transformations under applied magnetic field was considered.

Formation of ring structures from particles via dry hole formation on the wetting layers formed by the evaporation of a drop of particle colloid solution on the substrate is known [61]. The movement of particles on the substrate surface under the forces opening the hole and particle–substrate interactions are substantial points of the proposed mechanism for the ring formation [61]. Formation of micron and sub-micron size rings from amorphous $BaFe_{12}O_{19}$ superparamagnetic nanoparticles under the evaporation of a drop of colloidal solution on a carbon-coated Formwar copper grid was observed in Ref. [62] using TEM technique. In this case the interplay between interparticle magnetic forces and particle–substrate interactions was proposed to explain the structures observed. In our experiments the dry hole formation effect was most probably excluded because compressed ($\pi = 25$ mN m^{-1}) quasi-solid nanoparticulate surfactant monolayer was transferred to the substrate using conventional LB technique. Lateral movement should be stopped and nanoparticles should be fixed in such condensed molecular 2-D structure, therefore, the observed nano-rings were formed in the floating uncompressed Langmuir monolayer before its de-

position. The last was confirmed by our observations that the structure of deposited nanoparticulate samples was not changed after a few months of the sample storage under ambient conditions. Also, as it was shown in the present work, the shape of nanoparticles grown by the 2-D synthesis method can be substantially different for the same substrate and deposition procedure, but was strongly dependent on the nanoparticle growth conditions (monolayer composition and state, applied fields, metal and surfactant nature). On the other hand, the morphologies of nano-ring structures grown under the same conditions and investigated by AFM and TEM techniques were close (Figs. 1 and 5(e)). It also points out that the morphology of the nanoparticles obtained is determined by the processes of nanoparticles growth and self-organization in the monolayer and is rather independent of the deposition and sample preparation techniques. Nano-rings obtained in the present work via 2-D synthesis method are substantially smaller than other rings reported elsewhere. Kinetic factors and interparticle interactions including magnetic dipole–dipole interactions seem to be dominating in the mechanism of ring formation in the uncompressed floating monolayer in the absence of the particle–solid support interactions.

Nanoparticulate monolayers formed using 2-D synthesis method can be deposited using conventional techniques onto different solid substrates to form mono- and multilayer nano-composite LB films. Surfactants can be removed from such films by heating or using appropriate solvents with formation of layers of anisotropic nanoparticle aggregates with controlled thickness. Annealing of nanoparticulate films also can be used to control morphology of the product. Using appropriate solvents grown nanoparticles can be solubilized to form colloidal suspensions of highly anisotropic nanoparticles. Properties of such suspensions and colloid behavior of anisotropic nanoparticles can be interesting due to its shape anisotropy, and different from that of conventional spherical nanoparticles (as in electrorheological fluids and ferrofluids).

Concerning possible embodiments of the 2-D synthesis method it seems that many different metal-containing compounds could be used as precursors to produce anisotropic nanoparticles and nanostructures via this approach. The properties of such compounds should be the insolubility in the liquid phase and possibility to be included in the Langmuir monolayer. Generally, reactions of metal-complexes decomposition are rather complex and multistage, and the details of the mechanisms and kinetics governing many of the synthetic pathways are often not understood. Two-dimensional synthesis of nanoparticles described here may be useful for elucidation of fundamental mechanisms of such processes. Using appropriate combinations of precursors and other reagents anisotropic alloy, oxide and semiconductor nanoparticles can be obtained by this method. Controlling the mixed monolayer content, temperature and compression state along with the applied fields effects opens wide possibilities for regulation of the nanoparticles growth processes in the 2-D synthesis method to obtain anisotropic inorganic nanostructures with different and unique morphologies.

5. Conclusions

A novel approach for the synthesis of anisotropic nanoparticles and nanostructures is developed in which nanoparticles are fabricated via decomposition of an insoluble metal–organic precursor compounds in a mixed Langmuir monolayer at the gas/liquid interface. It is demonstrated that 2-D synthesis at the gas/liquid interface allows to produce anisotropic flatten inorganic nanoparticles with very high surface to volume ratio. The size and shape of magnetic nanoparticles can be changed from 2-D isotropic plate-like and ring-like to the field-aligned ellipsoidal when external magnetic field parallel to the plane of particulate monolayer was applied during the synthesis process. Controlling the morphology of nanoparticle-based nanostructures via anisotropic growth and interparticle interactions at the gas/liquid interface, intergrowth and coalescence processes under applied external fields, and by regulating the anisotropy and physical state of reaction media opens wide possibilities for regula-

tion the nanoparticles growth and self-organization processes to obtain anisotropic inorganic nanostructures with different predetermined and unique morphologies what could prove to be a promising approach for nanotechnology, nanophase engineering and creation of new nanostructured materials and ultrathin films with highly anisotropic physical–chemical properties.

Acknowledgements

AFM images were gratefully obtained by Dr R.V. Gainutdinov and Professor A.L. Tolstikhina, Institute of Crystallography RAS (Moscow). I thank Professor S.P. Gubin, Drs E.S. Soldatov, Yu.A. Koksharov, A.Yu. Obydenov for intensive and effective collaboration. This work was supported by Russian Foundation for Basic Researches (Grant 99-03-32218) and INTAS (Grant 99-864).

References

[1] G. Schmid (Ed.), Clusters and Colloids. From Theory to Applications, VCH, Weinheim, 1994.
[2] U. Kreibig, M. Vollmer (Eds.), Optical Properties of Metal Clusters, Springer, New York, 1995.
[3] Yu.A. Petrov, Clusters and Small Particles, Nauka, Moscow, 1986.
[4] J.H. Fendler, I. Dekany (Eds.), Nanoparticles in Solids and Solutions, Kluwer Academic, Doredrecht, 1996.
[5] A.P. Alivisatos, Science 271 (1996) 933.
[6] M.P. Pileni, J. Phys. Chem. 97 (1993) 6961.
[7] A. Taleb, C. Petit, M.P. Pileni, Chem. Mater. 9 (1997) 950.
[8] R.J. Davey, T. Hirai, J. Crystal Growth 171 (1997) 318.
[9] T. Hirai, J. Kobayashi, I. Komasawa, Langmuir 15 (1999) 6291.
[10] J.H. Fendler, F.C. Meldrum, Adv. Mater. 7 (1995) 607.
[11] M. Brust, D. Walker, D. Bethell, D.J. Schiffrin, R. Whyman, J. Chem. Soc., Chem. Commun. (1994) 801.
[12] X.K. Zhao, J.H. Fendler, Chem. Mater. 3 (1991) 168.
[13] N.A. Kotov, M.E.D. Zaniquelli, F.C. Meldrum, J.H. Fendler, Langmuir 9 (1993) 3710.
[14] K.C. Yi, V.S. Mendieta, R.L. Castanares, F.C. Meldrum, C. Wu, J.H. Fendler, J. Phys. Chem. 99 (1995) 9869.
[15] J. Yang, J.F. Fendler, J. Phys. Chem. 99 (1995) 5505.
[16] S. Mann, D.D. Archibald, J.M. Didymus, T. Douglas, B.R. Heywood, F.C. Meldrum, N.J. Reeves, Science 261 (1993) 1286.
[17] J.R. Thomas, US patent 3,281,344, 1966.
[18] J.R. Thomas, J. Appl. Phys. 37 (1966) 2914.
[19] C.B. Murray, D.J. Norris, M.G. Bawendi, J. Am. Chem. Soc. 115 (1993) 8706.
[20] P.H. Hess, P.H. Parker, J. Appl. Polym. Sci. 10 (1966) 1915.
[21] C.H. Griffiths, M.P. O'Horo, T.W. Smith, J. Appl. Phys. 50 (1979) 7108.
[22] E. Papirer, P. Horny, H. Balard, R. Anthore, C. Petipas, A. Martinet, J. Colloid Interface Sci. 94 (1983) 220.
[23] J. van Wonterghem, S. Morup, S.W. Charles, S. Wells, J. Villadsen, Phys. Rev. Lett. 55 (1985) 410.
[24] U. Netzelmann, J. Appl. Phys. 68 (1990) 1800.
[25] Y.S. Kang, S. Risbud, J.F. Rabolt, P. Stroeve, Chem. Mater. 8 (1996) 2209.
[26] V.F. Puntes, K.M. Krishnan, A.P. Alivisatos, Science 291 (2001) 2115.
[27] T.S. Ahmadi, Z.L. Wang, T.C. Green, A. Henglein, M.A. El-Sayed, Science 272 (1996) 1924.
[28] J. Zhu, S. Liu, O. Palchik, Yu. Koltypin, A. Gedanken, Langmuir 16 (2000) 6396.
[29] N. Herron, Y. Wang, M. Eddy, G.D. Stucky, D.E. Cox, K. Moller, T. Bein, J. Am. Chem. Soc. 111 (1989) 530.
[30] S. Joly, R. Kane, L. Radzilowski, T. Wang, A. Wu, R.E. Cohen, E.L. Thomas, M.F. Rubner, Langmuir 16 (2000) 1354.
[31] C.K. Preston, M. Moskovits, J. Phys. Chem. 97 (1993) 8495.
[32] Y.Y. Yu, S.S. Chang, C.L. Lee, C.R.C. Wang, J. Phys. Chem. B 101 (1997) 6661.
[33] S. Ravaine, G.E. Fanucci, C.T. Seip, J.H. Adair, D.R. Talham, Langmuir 14 (1998) 708.
[34] E.S. Smotkin, C. Lee, A.J. Bard, A. Campion, M.A. Fox, T.E. Mallouk, S.E. Webber, J.M. White, Chem. Phys. Lett. 152 (1988) 265.
[35] A.V. Nabok, A.K. Ray, A.K. Hassan, J.M. Titchmarsh, F. Davis, T. Richardson, A. Starovoitov, S. Bayliss, Mater. Sci. Eng., C 8–9 (1999) 171.
[36] M.M. Maye, W. Zheng, F.L. Leibowitz, N.K. Ly, C.J. Zhong, Langmuir 16 (2000) 490.
[37] G.B. Khomutov, A.Yu. Obydenov, S.A. Yakovenko, E.S. Soldatov, A.S. Trifonov, V.V. Khanin, S.P. Gubin, Mat. Sci. Eng. C 8–9 (1999) 309.
[38] D.K. Schwartz, J. Garnaes, R. Viswanathan, J.A.N. Zasadzinsky, Science 257 (1992) 508.
[39] G.L. Gaines, Insoluble Monolayers at Liquid–Gas Interfaces, Wiley, New York, 1966.
[40] B. Berkovsky, M. Krakov (Eds.), Magnetic Fluids and Applications—Handbook, Begel-House, New York, 1994.
[41] G.B. Khomutov, S.A. Yakovenko, T.V. Yurova, V.V. Khanin, E.S. Soldatov, Supramol. Sci. 4 (1997) 349.
[42] K.S. Suslick, S.B. Choe, A.A. Cichowlas, M.W. Grinstaff, Nature 353 (1991) 414.
[43] J. van Wonterghem, S. Morup, S.W. Charles, S. Wells, J. Villadsen, Phys. Rev. Lett. 55 (1985) 410.

[44] K.V.P.M. Shafi, S. Wizel, T. Prozorov, A. Gedanken, Thin Solid Films 318 (1998) 38.
[45] K. Esumi, M. Shiratori, H. Ishizuka, T. Tano, K. Torigoe, K. Meguro, Langmuir 7 (1991) 457.
[46] K. Esumi, M. Suzuki, T. Takafumi, K. Torigoe, K. Meguro, Colloids Surf. 55 (1994) 9.
[47] M. Brust, M. Walker, D. Bethell, D.J. Schiffrin, R. Whyman, J. Chem. Soc., Chem. Commun. (1994) 801.
[48] F.C. Meldrum, N.A. Kotov, J.H. Fendler, Chem. Mater. 7 (1995) 1112.
[49] G.B. Khomutov, E.S. Soldatov, S.P. Gubin, S.A. Yakovenko, A.S. Trifonov, A.Yu. Obidenov, V.V. Khanin, Thin Solid Films 327–329 (1998) 550.
[50] J.H. Fendler, Chem. Rev. 87 (1987) 877.
[51] N.R. Jana, Z.L. Wang, T. Pal, Langmuir 16 (2000) 2457.
[52] H. Majima, T. Hirato, Y. Awakura, T. Hibi, Metal. Trans. B 22 (1991) 397.
[53] A.V. Nabok, T. Richardson, C. McCartney, N. Cowlam, F. Davis, C.J.M. Stirling, A.K. Ray, V. Gacem, A. Gibaud, Thin Solid Films 327–329 (1998) 510.
[54] G.B. Khomutov, S.P. Gubin, Yu.A. Koksharov, V.V. Khanin, A.Yu. Obydenov, E.S. Soldatov, A.S. Trifonov, Mater. Res. Soc. Symp. Proc. 577 (1999) 427.
[55] T. Prozorov, R. Prozorov, Yu. Koltypin, I. Felner, A. Gedanken, J. Phys. Chem. B 102 (1998) 10165.
[56] T.C. Halsey, Science 258 (1992) 761.
[57] M. Sasaki, K. Haji, US Patent 5,523,157, 1996.
[58] T.F. Fujita, K.Y. Yoshino, US Patent 5,714,084, 1998.
[59] S.P. Gubin, A.Yu. Obydenov, E.S. Soldatov, A.S. Trifonov, V.V. Khanin, G.B. Khomutov, PCT International Patent WO 00/15545, Application RU99/00091, Published 23.03.2000.
[60] P. Jund, S.G. Kim, D. Tomanek, J. Hetherington, Phys. Rev. Lett. 74 (1995) 3049.
[61] P.C. Ohara, J.R. Heath, W.G. Gelbart, Angew. Chem., Int. Ed. Engl. 36 (1997) 1078.
[62] K.V.P.M. Shafi, I. Felner, Y. Mastai, A. Gedanken, J. Phys. Chem. B. 103 (1999) 358.